# ANNUAL REPORT 1978 ON

# MULTIPLE MIRROR PLASMA CONFINEMENT

by

A.J. Lichtenberg and M.A. Lieberman

Memorandum No. UCB/ERL M78/78

10 October 1978

ELECTRONICS RESEARCH LABORATORY

College of Engineering
University of California, Berkeley
94720

Research sponsored by the Department of Energy Contract EY-76-S-03-0034-PA215.

# *MULTIPLE MIRROR PLASMA CONFINEMENT*

# MULTIPLE MIRROR PLASMA CONFINEMENT


## Abstract

A large enhancement of the confinement time can be achieved in a straight system of multiple mirrors over an equal length uniform magnetic field. The scaling is diffusive rather than that of flow, thereby scaling as the square of the system length rather than linear with system length. Probably the most economic mode of operation for a reactor occurs when $\lambda/M \approx \ell_c$, where $\lambda$ is the mean free path, M the mirror ratio, and $\ell_c$ the length between mirrors; but where the scale length of the mirror field $\ell_m \ll \lambda$. The axial confinement time has been calculated theoretically and numerically for all important parameter regimes, and confirmed experimentally. A typical reactor calculation gives

$$\frac{P_{total\ electrical}}{P_{injected}} = 2$$

for a 320 meter system with 1500 MW(e) net output. A number of possibilities exist for improving this basic reactor performance.

Linked quadrupoles can theoretically achieve min-ave-B stabilization of flute modes, and experiments have demonstrated this stabilization. Feedback stabilization has also been shown to be possible, with experimental confirmation. Enhanced diffusion resulting from the distorted flux surfaces of min-ave-B has been investigated and shown to be manageable. Finite $\beta$ effects remain to be investigated.

# I INTRODUCTION

A multiple mirror device consists of a series of connected magnetic mirrors. In the appropriate plasma density and temperature regime for which the ion mean free path $\lambda$ is much less than the device length L, but long compared to the scale length of the changing magnetic field $\ell_m = B/(dB/dz)$, repetitive trapping and detrapping of ions by the multiple mirrors leads to a diffusive loss process[1-10] with the loss time scaling as $L^2$. For $\lambda > L$, free flow exists for untrapped particles with loss on a time scale $\tau \approx L/v$, where v is the particle velocity, while trapped particles are lost by the usual scattering into the loss cone. For $\lambda < \ell_m$ there is a gradual transition to MHD flow in which the loss time $\tau \approx ML/v$ where M is the mirror ratio. Viscosity effects preserve the $L^2$ diffusive scaling, although the fuil multiple mirror confinement time is not realized.[4,10]

In the next section we show that the multiple mirror loss time is given approximately by

$$\tau \simeq \frac{M^2 L}{2\lambda} \frac{L}{v} .$$

It is thus strongly enhanced over the free flow time if the mirror ratio is large and the mean free path is short. The mirror ratio is limited by magnetic field requirements and the requirement of $\beta = p/(B^2/2\mu_o) < 1$, where p is the plasma pressure and $B^2/2\mu_o$ the magnetic pressure. Considering that the mean free path is determined by classical collisions, the requirement that $\lambda$ be small suggests that the temperature should be as low as possible and the density as high as possible, since $\lambda \propto T^2/n$. To see this more clearly we note that the

power loss scales as $P_\ell \propto nT/\tau_{mm}$. Substituting for $\tau_{mm}$, $P_\ell \propto (T^{7/2} L^2)/M^2$. The fusion power, on the other hand scales as $P_f \propto n^2 f(T)$. For a reactor the optimum T is approximately 4.5 keV for a D-T Reaction. The density and mirror ratio M are chosen as high as possible, limited by available field strengths at $\beta<1$.

A number of options exist for major improvements in this basic reactor performance.[11,31] As examples: high Z material can be introduced to decrease the mean-free path; neutral beam injection with two-component operation can provide the benefit of additional fusion reactions; partial decoupling of the electron and ion temepratures can significantly increase performance. These concepts are discussed with respect to reactor design in Section V. If a process can be found in which $\lambda$ can be varied independently of classical collisions, then a more favorable reactor scaling exists, leading to a higher optimum ion temperature and considerably lower field and length requirements.[12] In this case $P_\ell \propto T^{3/2}$ and $T_{opt} \approx 14$ keV. The length, magnetic field, and total power depend on assumptions of the nonclassical scattering process, which is discussed in greater detail in Section V and Ref. (12).

A two-component ("wetwood burner") reference reactor design, summarized in Section V, gives the following results. Typical reactor parameters are: length L=320 m, $T_e$=6 keV, $T_i$= 4.5 keV, density $n=7.7 \times 10^{15}$ cm$^{-3}$, and plasma pressure = 290 bar, with net electrical power output $P_{net}$= $P_{recirculating}$. There are seven cells. For $P_{net}$=1500 MWe, the plasma diameter is 3 cm. For $\beta$=.8, the solenoidal field is 9.3 T and the mirror field is 14 T. The 180 keV neutral beam injection current is 8.3 kA. The breakeven reactor $P_{net} \approx 0$ at the same magnetic field strength would have $T_e \approx 3$ keV and reactor length L≈35 m.

In contrast to the wetwood burner solution, a reactor design of roughly the same Q and length, but employing the beam mainly for supplying energy, would have a magnetic field approximately 1.7 times as large to take up the pressure.

An alternative approach is to allow $\beta>1$ with the pressure taken up by a gas blanket and radial diffusion inhibited by the residual field. This approach is actively being pursued by the Novosibirsk group.[9] In the Novosibirsk high $\beta$ configuraton, as in a proposal by Tuck[10] for confinement of a $\beta=1$ plasma, the magnetic moment $\mu$ is not conserved. However, another adiabatic invariant exists which acts similarly to the $-\mu\nabla B$ force to reflect particles. The reflections occur where the plasma diameter narrows due to the external mirror field. Tuck did not consider collisions, but rather discussed the possibility that the external field could be made to vary sufficiently fast that adiabaticity is lost, thus simulating the effect of fixed scattering center collisions.

As an endstoppering mechanism, multiple mirrors can also be incorporated into other reactor concepts. These include steady state or pulsed reactors driven by intense electron beams, ion beams or lasers. For example, with an axial electron beam injection at 100 keV, one would require $3\times10^4$ amperes of electrons, steady state. It has been shown that, even in the absence of strong collective effects, a 100 keV electron beam will collisionally transfer most of the energy along a plasma column of the density and length of the proposed reactor.[27] Studies of energy absorption for MeV beams in multiple mirrors are being pursued, among other places, at Physics International,[28,29] and at Novosibirsk.[90] A pulsed linear $\theta$-pinch reactor may also be stoppered, in principle, with multiple mirror end sections. Details

of reactor configurations of these types, including stabilization for the mirror sections, have not been explored.

In common with toroidal devices, multiple mirror containment is at best average minimum B, and therefore subject to localized modes.[14] At high $\beta$, the connection lengths for localized mode suppression are small, but reactor designs can conveniently minimize the connection length. Drift instabilities would be expected to enhance radial diffusion, which can be serious in these naturally small diameter systems. If linked quadrupole stabilization is used the field line fanning will also enhance radial diffusion. These problems must all be considered carefully in evaluating the multiple mirror concept. Because the loss cone is nearly full, the multiple mirror should not be subject to velocity space instabilities.

In Section II we will review the theory of multiple mirror confinement, and the results of computations. Stability theory will be considered in Section III, and in Section IV the results of experiments confirming the multiple mirror scaling laws and stability theory will be reviewed. Reactor calculations will be given in Section V.

# II CONFINEMENT

## A. *Axial Loss*

We present here a simple treatment of the axial diffusion process, emphasizing the basic mechanism for confinement. Consider a symmetric multiple mirror system with F particles per unit area per unit time injected into the center in the steady state. The mirror widths $\ell_m = B|dB/dz|^{-1}$ are assumed to be small compared to $\ell_c$, so that the loss cone angle $\theta_c$ defined by $\sin^2\theta_c = 1/M$, where $M \equiv B_{max}/B_{min}$ is the mirror ratio, is a constant over the cell length $\ell_c$. For many cells ($L \gg \ell_c$) large mirror ratios ($M \gg 1$), and sufficient source strength F such that the scattering mfp $\lambda \ll L$, particles will be trapped and untrapped many times before reaching the ends, so that their axial motion can be described by a random walk.

Since the distribution of velocities in such a system may approach Maxwellian, the scattering distances for individual particles vary from distances much less than $\ell_c$ to distances much greater than $\ell_c$. Considering the velocity groups which would have average step length $\ell_z \gg \ell_c$ (but $\ell_z \ll L$), the average step length $\ell_z$ and step time t can be estimated from average times $t_1$ and $t_2$ spent out and in the loss cone, respectively. For particles at speed v, and $M \gg 1$ (small $\theta_c$) we can estimate

$$t_2(v) \approx \tau_\theta(v)\theta_c^2 \approx \frac{\tau_\theta(v)}{M} \qquad (1)$$

where $\tau_\theta(v)$ is the scattering time at speed v for a mean-square deflection of $\theta = 1$ radian. We define the average step length between successive trappings to be

$$\ell_z(v) = \alpha t_2(v) v \approx \frac{\lambda}{M} \tag{2}$$

where $\alpha$ is a proportionality constant of the order of unity which can be determined by a more exact theory or by experiments.

Assuming the velocity-space density of ions at speed v in th loss cone is nearly the same as that out of the loss cone, (e.g., a Maxwellian) statistical mechanics gives the ratio of trapped time $t_1(v)$ to untrapped time $t_2(v)$ (see Ref. 1) equal to the ratio of trapped to untrapped surface area at radius v in velocity space

$$\frac{t_1(v)}{t_2(v)} = \frac{\cos\theta_c}{1 - \cos\theta_c} \approx 2M \qquad (M \gg 1) \ . \tag{3}$$

Equation (3) was found qualitatively to describe numerical results for $\frac{t_1}{t_2}$ (see Ref. 1). For large M, $t_2(v)$ can be neglected compared to $t_1(v)$ in the total step time $t(v)=t_1(v)+t_2(v)$, and Eq. (3) with Eq. (2) gives $t(v)\approx 2\tau_\theta(v)$. Note that for $\alpha$ of order unity and $\ell_z(v) \gg \ell_c$, $t_1$ is many bounce periods $\ell_c/v$, so that the concept of trapping is well-defined. In this limit we can define a diffusion coefficient for the average velocity $\bar{v}$, satisfying $\ell_z(\bar{v}) \gg \ell_c$, as

$$D(\bar{v}) \equiv \frac{\ell_z^2(\bar{v})}{2t(\bar{v})} \simeq \frac{\lambda\bar{v}}{4M^2} \tag{4}$$

For $\ell_z/\ell_c \ll 1$ the cell length $\ell_c$ is the basic step size and a straightforward analysis yields[7]

$$D_{min}(\bar{v}) = \frac{\ell_c\bar{v}}{4M} \tag{5}$$

where the subscript *min* refers to the minimum diffusion coefficient at a fixed $\ell_c$. If this relationship holds for most particles in all cells, then the density profile is triangular; $dn/dz = \text{constant} \equiv 2n_1/L$, with an average density $n_a = n_o/2$. For a discrete system of $N = L/2\ell_c$ cells in a half length L/2, the maximum density $n_1$ in the center cell is given by $n_1 = N\delta n$, where $\delta n$ is the density increment across each mirror. The containment time for this case is

$$\tau_{mm}(max) = \frac{n_1 L}{2\bar{D}_{min}\nabla n} = \frac{ML^2}{2\ell_c \bar{v}} \quad . \tag{6}$$

A number of theoretical treatments have been devised, valid for both of these limits, as well as for the transition between them, giving essentially the results indicated here.[4,6] In addition to calculations of the particle flux $F = -D\nabla n$, the end loss energy flux G can also be calculated. Defining $\lambda^* \equiv \lambda/M$, if we take the product $|(G\bar{D}_{min})/(kTF\bar{D})|$ to obtain the relative variation of G as a function of $\lambda^*/\ell_c$ we find that the product has a broad flat region near $\lambda^*/\ell_c = 1$, rising slowly for $\lambda^*/\ell_c < 0.2$ and falling flowly for $\lambda^*/\ell_c > 5$. Considering that the system length L and $\lambda^*$, are held fixed, we obtain the result that the energy flux decreases slowly, i.e., the energy confinement time increases slowly with increasing number of mirrors. The limiting case is the corrugated magnetic field strucuture.[3,4] For economy of design, long mirrors are desirable, and we therefore will concentrate our attention on the region for which $\lambda^*/\ell_c \gtrsim 1$.

The high density regime needs to be looked at separately, however, for if $\lambda \ll \ell_c$ then it may also be that $\lambda < \ell_m$. In this case the magnetic moment is not constant in the mirror region and ion flow is limited by ion

viscosity. For this regime Mirnov and Ryutov[4] and Berk[10] obtain multiple mirror loss times of the form

$$\tau_{mm} = \frac{f(M)L^2}{2\ell_c v}\frac{\lambda}{\ell_m} \tag{7}$$

where f(M) depends on the exact form of the magnetic field. Thus, the confinement time is reduced proportional to $\lambda/\ell_m$ for increasingly short mean free paths. For a variety of magnetic field shapes we find $f(M) \propto (M-1)^2$, and thus the $M^2$ mirror ratio scaling is recovered for large M. Comparing Eqs. (4) and (5) with Eqs. (6) and (7) we observe that with L and $\ell_c$ fixed, the multiple mirror diffusion time is maximized for $\ell_m < \lambda < M\ell_c$. For collosional scattering, in which $\lambda \propto 1/n$, in order to remain in the optimum range over many cells, we require that $\ell_m \ll M\ell_c$. This inequality is found to be consistent with stability considerations.

Except where explicitly noted, the above analysis is independent of the scattering mechanism. For collisional scattering $\lambda \propto T^2/n$ which is then used for optimization of parameters in reactor calcuations in Section V. However, there are mechanisms such as nonadiabatic scattering for which $\lambda$ may have entirely different n and T dependencies.[12] In Section V-F we show how other scalings can lead to more favorable reactor parameters.

Numerical calculations of containment time in a multiple mirror device were made using a model in which the field particle densities, drift velocities and temperatures are included in a self-consistent manner.[6] A number of test particles are numerically followed through the multiple mirror system with the velocity vector of each test particle varied on each step. The variation is composed of two parts, an adiabatic change due

to the variation of the magnetic field and a random change arising from small angle Coulomb sollisions with the background plasma. The random small angle scattering is computed in the center of mass frame of the background plasma which is drifting, and the velocity vector transformed to the laboratory frame for computation of the adiabatic motion. The mathematical procecure is presented in Ref. (1) and (6). The confinement times of a large number of test particles are averaged to obtain a multiple mirror confinement time. The mirror regions were peaked in accordance with the theory and also to simulate actual reactor designs. The results confirmed both the $L^2$ scaling and the value of the containment time predicted from the theory with $\lambda^* \approx \ell_c$ at the average density.[6]

In the preceding analysis, one important factor that has not been taken into account is the electrons. The electrons diffuse more rapidly than the ions by the ratio M/m and thus are contained by an amibpolar force reuiqred to preserve charge neutrality. As the electrons are in thermal equilibrium with the ions they increase the axial diffusion by a factor of two. Heat conduction must also be considered. This is rapid compared to the ion containment time within the multiple mirror system and therefore keeps the temperature constant. At the machine ends care must be taken that cold electrons are not available to reenter the device exchanging energy with the hot trapped electrons. This problem, common to mirror devices, is generally thought to be accomplished by expansion of the field lines, which would be required, in any event, if direct conversion is employed. Although there is considerably higher density in multiple mirror devices than in single mirrors, the density in the end cells of the multiple mirror is approximately 1/N smaller than that of the central cells. These issues are considered in Section V.

## B. *Radial Diffusion*

We next consider, briefly, the problem of radial diffusion. If the primary mechanism is the amibpolar electron-ion diffusion, then for reaonable dimensions and parameters the radial loss is negligible compared to the axial loss. However, when the ratio of the ion gyroradius to the plasma transverse dimension is of order of the fourth root of the mass ratio, then calculations indicate that like-particle diffusion becomes significant.[15] This situation can occur because the device is operated at high $\beta$, the plasma radius is reduced to a minimum value to reduce the total system power or the plasma is distorted to a highly noncircular shape by quadrupolar stabilization. These factors can act together, but are counterbalanced by the fact that tha plasma $\beta$ is reduced in the mirror throats where the radial scale length, particularly in the quadrupole stabilized system, becomes smallest. In a typical reference reactor design, moreover, the fanned regions constitute a small fraction of the axial length and thus the diffusion in the fans may be the highest per unit length and yet not be dominant.

We can compare classical radial and axial diffusion using calculations of radial diffusion from Ref. (15). For a cylinder with uniform axial density the eigenvalue problem for like-particle radial diffusion was solved to obtain a radial time constant

$$\tau_r = \frac{8\pi r_p^4}{12 a_i^4} \tau_{ii} \qquad (8)$$

where $a_i$ is the Larmor radius and $r_p$ the plasma radius. If we assume that the lengths and mirror ratios of the cells are designed to maintain the optimality of the axial containment, we may take $\tau_{ii} \approx M\ell_c/\bar{v}$, and Eq. (6) then becomes

$$\tau_{mm} = \frac{L^2}{2\ell_c^2}\tau_{ii} \quad . \tag{9}$$

Comparing Eqs. (8) and (9) we find that $\tau_r \geq \tau_{mm}$ for

$$\frac{r_p}{a_i} \geq \left(\frac{L}{2\ell_c}\right)^{\frac{1}{2}} . \tag{10}$$

For the reactor example in Section V, with T=4.5 keV, B=9.3 T, $\beta$=.8, $r_p/a_i \approx 4$ and since $L/2\ell_c \approx 5$, Eq. (10) is satisfied. In this design the diffusion in the fans is negligible because the decrease in the narrow dimension of the fan is more than compensated by the decrease in $a_i$ due to the combination of increasing B and decreasing $\beta$.

Estimates have been made of the effect of neo-classical diffusion due to the nonaximsyymetry of the flux surfaces.[16] Due to the collisional natures of the plasma these effects appeared to be small, but a complete calculation of the motion on the actual J surfaces has not been made. Pseudoclassical and nonclassical diffusive processes have not been explicitly considered. However, we have estimated that for the parameters used in the reactor design noncollisional radial diffusion of the order of $10^{-3}$ $D_B$(Bohm) would be acceptable.[7] We also note that the radial diffusion does not lead to actual radial loss, but to enhanced axial loss at large radii. This is due to the onion-skin effect in which axial diffusion increases

at large radii because the density is reduced.[17] Thus, the radial and axial fluxes combine and can be considered as a total particle flux for purposes of direct conversion.

The radial diffusion problem is considerably different, if we consider diffusion due to the nonadiabaticity of the fields. In this situation, in the worst case, a cross-field scattering occurs with each axial scattering, such that the condition that $\tau_r = \tau_{mm}$ becomes

$$\frac{r_p}{a_i} \approx \frac{L}{M\ell_c} . \tag{11}$$

This leads to requirements of a much larger plasma radius and higher power/unit length. However, for axisymmetric magnetic fields the existence of the canonical angular momentum as a constant of the motion prevents radial diffusion, and Eq. (11) need not be fulfilled. For nonadiabatic scattering a strong premium is therefore put on stabilization with axisymmetric fields. We are currently investigating if there are conditions for which an adiabatic invariant exists, to prevent radial diffusion in linked quadrupole stabilized fields, without axisymmetry.

# III STABILITY

## A. *Minimum-Average-B*

A magnetic configuration consisting of magnetic mirrors and linked quadrupole fields can produce a min-ave-B well in a region near the axis.[18] Optimization procedures have been employed, using the Euler-Lagrange Equations, to determine the parameters that give minimum ellipticity for marginal stability, and give the largest region of stability.[19] Minimum values of ellipticity for marginal stability as a function of R/L (where $R \approx \ell_m$) and M are given in Fig. 1. Here R is the mirror coil radius. A broad optimum near the maximum region of stability was found near the values of $M = 4$ and $R/\ell_c = 0.1$ for the mirror field. Assuming a realizable form for the mirror field, the maximized stable radius at the midplane, $r_w$, is given as a function of the ellipticity, Q, in Fig. 2. Above $Q = 20$ a broad maximum of $r_w/R \approx 15\%$ exists. These values are quite consistent with typical parameters of our reactor calculation for which $r_w = 3$ cm, $R \approx 50$ cm and $\ell_c \approx 5$ m. The ellipticity of 20 leads to enhanced but still acceptable radial diffusion, as discussed in the previous section.

Practical coil designs approximating these optimized fields can be constructed for experiments, consisting of mirror and solenoidal fields and weak and strong quadrupole currents, the weak currents extending over the entire cell, while the strong currents extend only in the neighborhood of the mirrors. A comparison of the results of the practical coil design with the results from the optimized equations is given in Fig. 3. Here $r_{min} = r_w/MQ$ is maximized, to minimize diffusion in the fans ($r_w/R \approx .15$,

as before). Experiments on a multiple mirror device, to be described in Section IV, were performed with linked quadrupole coils that had not been optimized, and for which min-ave-B was not obtained. A 10 meter multiple mirror device is currently under construction which employs the optimized coil configurations. The optimized values of $M = 4$ and $R/\ell_c = 0.1$, used in the design, also allow the intermediate mean free path to be maintained over a wider range of densities, thus allowing a more exact comparison of theory and experiment in the 10 meter device. The parameters of the large experiment are given in Table 1.

One limitation of min-ave-B stabilization is the onset of localized modes with finite $\beta$. A criterion for stability against these modes [14]

$$\beta_c \leq \frac{8\pi^2 \gamma r_p R_c}{\ell_m^2} \tag{12}$$

where $\gamma$ is a ratio of average good curvature to the characteristic curvature $R_c$, $r_p$ is the plasma scale length and $\ell_m$ the connection length. Although it is difficult to calculate these quantities outside of a specific design, we estimate that $\gamma \approx 1/10$, $r_p R_c/\ell_m^2 \approx 1/10$ such that $\beta \approx 1$. Furthermore, the region of bad curvature occurs where the field is maximum, and therefore where $\beta$ is minimum. We expect, therefore, that substantial $\beta$'s are possible in realistic reactor geometries.

The fan shaped flux surfaces that are created by min-ave-B coils have a number of undesireable features, some of which have already been mentioned. They enhance the radial diffusion due to collisions, and break the $p_\theta$ invariant that would otherwise prevent radial diffusion arising

from nonadiabaticity. In addition, as described in Section V-G they increase the Joule heating in the nonsuperconducting mirror and strong-quadrupole coils and increase the complexity of coil design and construction.

### B. *Feedback and Other Stabilization Methods*

Although a major effort has been devoted to min-ave-B stabilization, other methods of stabilization not requiring distorted magnetic surfaces may be possible. These include feedback, line-tying, dynamic, and wall current stabilization. The small radius of a multiple mirror plasma indicates that few modes would be present, which makes feedback stabilization quite attractive.

Axial feedback stabilization of the flute mode in a mirror-confined plasma of density $n_o$ has been considered for stabilization of a multiple mirror.[20] The instability is described using the usual low frequency slab model. The instability potential $\phi$ is sampled at various azimuths around the plasma circumference. The sampled potential is amplified, phase shifted in azimuth, and the resulting feedback voltage e is applied to a conductin endwall split into azimuthal segments. An external plasma of density $n_x$ is present in the region between the confined plasma and the endwall. The admittance between the endwall and confined plasma is modeled to include the external plasma impedance and the sheaths at the endwall and mirror throat. For typical multiple mirror reactor conditions stabilization is obtained for exactly 90° azimuthal phase shift provided $en_x/\phi n_o$ is greater than $7m^2a_i^2/r_p^2$, where p is the azimuthal mode number, $a_i$ the ion Larmor radius, and $r_p$ the plasma radius. For $m = 1$, $a_i/r_p \approx 0.1$, and

$n_x/n_o \approx 10^{-2}$, the required gain $e/\phi$ for stabilization is modest. By sampling the potential and its derivative, or by sampling the time integral of the potential, feedback stabilization is obtained over a wide range of azimuthal phase shift angles, as shown for integral feedback stabilization in Fig. 4. Studies of finite time delays and mode coupling in the feedback loop have been performed. Time delays lead to a transcendental equation which was solved using finite sample time, z-transform techniques. The delay leads to a shrinking of the teardrop-shaped region of stability shown in Fig. 4. The flute modes are coupled by the inhomogeneous (discrete) nature of the probe sampling system and the end collector feedback plate system. The coupling is being studied using a system-theoretic matrix approach in which the input-output matrices for all elements in the feedback loop are separately modeled, including all effects of mode coupling, line-tying, and finite Larmor radius. The theory shows that stable or weakly unstable higher order modes can be driven more unstable in the process of stabilizing the m = 1 mode, due to mode coupling, and that this effect can be eliminated if the sampling system properly decouples the modes. An experiment in which the m = 1 flute mode was successfully stabilized by means of integral feedback is described in Section IV-C.

An initial analysis of wall current stabilization indicates that the method can be effective in suppressing flutes. Alternating the stabilization current can prevent the appearance of current driven modes. A calculation for reactor parameters indicated stabilization with an oscillating current of 5 kA, well below the random current.[21] Comparison of currents in a long thin mirror system with the dynamic stabilization currents needed in Scyllac show that this current is an order of magnitude

less than would be required to dynamically stabilze a toroidal device.[22] The requirement of having a close wall may be a difficulty with this scheme. The stabilization scales in such a manner that it is difficult to test the method on a small experiment.

# IV EXPERIMENTS

## A. *Line-Tied Axial Confinement Experiments*

Because the mean free path scales as $\lambda \propto T^2/n$ it is possible to scale laboratory size experiments over a wide range of temepratures and densities while maintaining $\lambda \approx \ell_c$. A convenient steady state plasma can be created with a "Q-machine" source. Experiments with this type of source have been carried out at Berkeley[5,7] and at Novosibirsk.[8] The steady-state plasma generated at a hot plate simulates a central source for a multiple mirror device, with the length of the experimental system being one half of a symmetrical device. Simple magnetic mirrors can be used in this configuration, as the plasma is stabilized by line-tying to the hot plate. The effects of neutrals can be made negligible, but recombination at the hot plate, as well as radial loss, must be considered.

The Berkeley device (Fig. 5) contained a series of water-cooled coils forming up to 8 mirror cells along a 6 cm in diameter, 150 cm long vacuum chamber. The peak magnetic field is in the 5 kG range and the mirror ratios could be varied between 1 (nearly uniform) and a large number (say 10) depending on the coil configuration. The plasma length was varied by moving a negatively biased collector plate along the chamber axis, as shown in Fig. 5. The end loss rate of ions was measured by the collector current $I_c$. The number of mirror cells $N = L'/\ell_c$ was varied either by moving the collector within a fixed multiple mirror field, or by switching mirrors on and off between the source and a fixed collector. The plasma density was

measured by Langmuir probes which could be moved both radially and longitudinally to explore the entire plasma volume. A comprehensive set of experiments has been performed confirming the variation of confinement time with the square of number of cells and the predicted variation with average mirror ratio. The stepwise density falloff from cell to cell as well as the stepwise increase in density in the first cell as new cells were added, were also demonstrated. The experimentally determined values of the confinement time were also in reasonable agreement with those expected from the theory. The transitions to the free flow regime at low density and to the MHD flow regime at high density were also demonstrated.[7]

Here we give examples from some of the results. In Fig. 6, we compare the density profile for a long mirror with a three cell system of the same overall length. Figure 6a shows the density profile at low density indicating the free flow behavior in which the density follows the magnetic field variation. In Fig. 6b, the density has been increased to the intermediate mean free path regime in which the increased density in the first cell and the characteristic stairstep density pattern is observed. The ratio of confinement times of 2, between the multiple mirror and the long mirror configurations is as predicted by the theory.

Another test of the scaling law of multiple mirror confinement time with the number of mirror cells can be made by observing the changes in the density in the first cell, $n_1$, for a constant source, as the collector is withdrawn within a fixed multiple mirror field, thus adding mirror cells to the system. Figure 7 shows the probe current (density) in the first cell next to the source as a function of collector position in the (a) low, (b) intermediate, and (c) high density regimes. In Fig. 7b

the density at the source is seen to increase in a stepwise fashion as the collector passes each mirror throat, adding another cell to the system. The increase in density is strongest in the intermediate density regime, as expected. The first density jump, corresponding to the collector passing the second mirror is a result of particle filling of velocity space due to ion trapping when the first cell is created, and is not a multiple mirror effect.

The Novosibirsk device[8] had 13 mirrors over a 2 meter length and could be switched between a uniform field and a mirror ratio of M = 1.83 with $B_{max} = 5{,}400$ Gauss. The device operated in a density range for which $\lambda^* > \ell_c$ such that the axial density distribution should vary exponentially. Comparison of the density in the last cell, $n_L$, with the density in a cell, nine cells closer to the source, $n_9$, gave increasing ratios of $n_9/n_L$ as the density was increased, indicating that gradual transition from the free flow to the multiple mirror regime. At the highest density of stable operation they obtain $n_9/n_L \approx 4$, which was in good agreement with the theoretical value of $n_9/n_L = 9/2\ell n 9 = 4.3$. Switching to a uniform field gave $n_9/n_L = 1$, as expected. They also operated in a transient (but still line-tied) mode by intercepting the neutral flux before it reached the hot plate. The increase in the transient plasma lifetime with increase in plasma density was consistent with that expected from increasing multiple mirror action.

### B. *Transient Experiments*

The Berkeley multiple mirror device was modified to include linked quadrupole fields in an attempt to achieve min-ave-B stabilization.

The basic design follows principles described in Section III-A and Refs. 18 and 19. Practical constraints of coil size, mirror lengths, and external leads, altered the design shape sufficiently that min-ave-B could not be attained. Subsidiary trim coils (arc straps) designed to counteract the adverse effects of the leads, which weaken B where the curvature is unfavorable, did not fully counteract these adverse effects. In the final design the unfavorable average curvature was improved by a factor of 2 at one half centimeter radius, in the compensated system. The ellipticity is approximately 10 in this design. The magnet and quadrupole configuration is given in Fig. 8.

Transient experiments to test both confinement and stability, have been performed in two density and temperature ranges.[23,16] In the first, a gating coil creates a cusp field between the multiple mirrors and the hot plate to eliminate both the source of new plasma and the line-tying. Without the quadrupole fields the plasma becomes flute unstable and moves transversely to the walls. Despite the lack of complete compensation, there is a range of parameters in which at least partial stabilization can be obtained.

The decay of plasma density was observed both with Langmuir probes and with a plasma camera. The latter device could be used both to identify the modes and to observe that rate of translation of the plasma for the $m = 1$ mode. In Fig. 9 a typical set of sequential plasma camera pictures are shown for a given mirror ratio and three values of stabilizing quadrupolar field. The plasma is observed to move mainly in an $m = 1$ mode with some indication of $m = 2$ and higher modes. The $m = 1$ flute velocity is substantially reduced with the quadrupolar fields. Similar pictures for other mirror ratios

indicated increasing instability with increasing mirror ratio. The growth rate in its simplest form is given by

$$\gamma = \left(\frac{2\bar{v}^2}{R_c}\ \frac{1}{r_p}\right)^{\frac{1}{2}} = \sqrt{2}\left(\frac{\bar{v}}{L_B}\right) \tag{13}$$

where $L_B$ is the magnetic field scale length and $\bar{v}$ is the ion thermal velocity. We therefore expect both the growth rate and the large amplitude drift to be proportional to $L_B^{-1}$. In Fig. 10 the measured flute velocity is plotted against $L_B^{-1}$ for varying both the mirror ratio and stabilizing the field. All points lie on a single curve, indicating the importance of the $L_B^{-1}$ driving term, but the dependence is closer to $L_B^{-2}$ with apparent stabilization at finite $L_B^{-1}$ indicating the presence of other stabilizing mechanisms. The decay time under stabilized conditions was of the order of 1 msec compared to an estimated theoretical decay time of 1.5 msec.

In the second experiment a higher density and temperature transient plasma was created by a conical θ-pinch source. Keeping $\lambda \propto T^2/n$ constant, the temperature was scaled up by almost two orders of magnitude to $T \simeq 10$ eV, and the density scaled correspondingly by almost $10^4$, to $n \simeq 10^{14}$. This temperature range with a density of $10^{15}$ (required to allow for expansion into the multiple mirror) was achieved with a 50 kV, 2 μf capacitor at a filling pressure of $\tilde{\sim}$20 Torr of hydrogen. The gas fill was accomplished with a pulsed gas valve to keep the main system at low pressure, with a 50 cm uniform magnetic guide field used to separate the neutrals by time-of-flight (400 μsec) from the experiment which has a characteristic decay time of about 100 μsec. An additional fast gating coil can be used to prevent

the influx of slower plasma. The experimental results were similar to those at low temperature and density, showing an onset of stabilization with increasing quadrupole current. Axial profiles of density are shown in Fig. 11. Detailed measurements of this nature have been made and compared with a simulation model of the buildup and decay process, showing reasonable agreement for the stabilized plasmas.[16]

We observed that the decay times from the simulation $\tau_{sim}$ were higher than the experimental decay $\tau_{exp}$ by 30% to 60%. The main reason for this discrepancy is probably the enhancement of the ion diffusion caused by the electrons, which tend to leave the mirror system axially at a higher rate than the ions (the numerical model ignores electron effects).

A second observation concerns the classical radial losses. The reduction in confinement time due to enhancement in classical radial loss by the ellipticity in the fans at a given mirror ratio, for the simulation, is 11% at M=1.6 and 20% at M=2.2. For the experiment, these figures are 15% and 29%, respectively. We consider that the radial losses calculated in Ref. 15 are in reasonable agreement with the experimentally observed radial losses. We note that the observed radial losses correspond to a maximum of a few percent of Bohm diffusion and, thus, the level of turbulence in those experiments is limited to a few percent of the Bohm value. Neoclassical diffusion, arising from particle drifts in the nonaxisymmetric fields, has been estimated to be at least a factor of 10 below the ion-ion radial diffusion and, therefore, could not be osbserved in these experiments.

A number of reasons may be advanced for the improvement of stability over that predicted from MHD theory. Although finite Larmor radius effects theoretically do not stabilize the m = 1 mode in azimuthally

symmetric systems, they may have an effect in the strongly fanned configuration, particularly as the stabilization was more pronounced in the hotter plasma in which there are only two to three Larmor radii across the narrow dimension of the ellipse. A related stabilizing effect from nonuniform plasma rotation could arise from ambipolar electric fields.

The most probably explanation for the enhanced stability is residual line-tying. Calculations, including line-tying, have been made which indicate that, for the amount of external plasma estimated to be present, the growth of the M = 1 mode can be sufficiently slowed to stabilize the plasma during the lifetime of the experiment.[24] This conclusion holds both for the alkali and for the hydrogen plasmas. The residual line-tying can also destabilize higher order modes, a situation that was also observed in the experiments.[23]

## C. *Axial Feedback Experiments*

Although line-tying, by itself, is probably not practical for fusion plasmas, we recall from Section III-B that line-tying coupled with feedback may be a viable alternative to min-ave-B stabilization. Axial feedback stabilization has been successfully employed on the Berkeley multiple mirror device using the low temperature lithium source.[32] Simple mirrors without the linked quadrupole windings were employed. A set of eight Langmuir probes arranged azimuthally around the circumference of the plasma, a set of eight probe current amplifiers, an end collector split into four segments, and four feedback amplifiers with adjustable amplitude and azimuthal phase were constructed and employed in the experiment. In the absence of

the feedback signal, the m = 1 flute mode was seen to appear when the source gating coil was fired, disconnecting the plasma from the hot plate. The plasma was lost radially to the wall, as shown in Fig. 12a. With the feedback present and properly adjusted in phase and amplitude, the instability was absent and the plasma decayed smoothly with a lifetime of approximately 1 msec. This decay is seen in Fig. 12b. Theory and experiment are in good agreement.

Recently, a mode decoupler has been constructed which allows separate and simultaneous observation of the m = 1,2 and 3 mode amplitudes vs time. Preliminary stabilization experiments using this decoupler have been performed, in which the m = 1 flute mode was stabilized without affecting the higher order mode amplitudes. Qualitative agreement between theory and experiment has been obtained. The experiments are continuing.

### *D. The Ten Meter Experiment*

The parameters of the ten meter multiple mirror experiment are given in Table 1. Detailed calculations of field line shapes were made using the MAFCO code, and the min-ave-B properties of the field structure was confirmed. A mechanical design was developed, and a prototype cell was built. An electron source was used to map out the magnetic flux suefaces. It was found that considerable distortion in the flux surfaces was introduced by the mechanical design. Field line calculations were extended to include various types of field errors, so that these errors could be predicted. Redesigned sets of one, three, and five cell systems were tested to determine field alignment procedures and the use of the compensation windings. Satisfactory results were obtained.

In Fig 13a photographs of flux surfaces at various axial positions in a cell are shown as taken by the plasma camera. In Fig. 13b the theoretical and actual flux surfaces are shown after passing from midplane to midplane through three cells of a five cell system, showing the dipole field distortion before and after applying the correction fields. The entire system has been constructed employing the revised mechanical design. A single cell is shown in Fig. 14, giving the main features of solenoid and weak quadrupole bars, and with the mirror and strong quadrupole embedded in fiberglass epoxy to withstand 20 kG stresses. Electrical tests of the system and the theta pinch source are currently under way. The experiments are continuing.

# V REACTOR FEASIBILITY

## A. *Basic Reactor*

Preliminary evaluations of the significance of the multiple mirror concept have been made by estimating parameters for steady state reactors, assuming synchrotron radiation, radial diffusion, and axial and radial heat flow losses are negligible. Both beam-driven DT and wet-wood burner configurations have been considered. The energy flows considered are fusion neutrons $P_n$, fusion alphas $P_\alpha$, bremsstrahlung power loss $P_\beta$, and power loss associated with plasma loss along field lines $P_\ell$. Taking a practical magnetic field limit $B_{max}$ in all mirror throats, the midplane field is chosen to maintain the plasma $\beta$ constant, which allows for the maximum mirror ratio in each cell.

We assume $P_n$ and $P_\beta$ are converted into electricity by a thermal cycle at efficiency $\eta_T$, $P_\alpha$ is deposited directly within the plasma, and $P_\ell$ is directly converted into electricity at efficiency $\eta_{DC}$. The reactor Q is defined as

$$Q \equiv \frac{P_f(\textit{fusion power})}{P_b(\textit{injected, or recirculating electrical power})},$$

and the power ratio $Q_E$ is defined as

$$Q_E \equiv \frac{P(\textit{total electrical power generated})}{P_b(\textit{injected, or recirculating electrical power})}.$$

For $P_{net} \geq 0$, $Q_E \geq 1$, the recirculating electrical power fraction is $Q_E^{-1}$.

One possible method of supplying the recirculating energy is by high energy neutral injection transverse to the device. An additional benefit is the power produced by hot deuteron warm triton fusion reactions. Computational studies of energy balance have been undertaken[11, 31] in order to investigate reactor parameters available under two-component operation. A simplified reactor model was considered to explore the effects of two-component operation and impurities, rather than to economically optimize reactor parameters. Variable length mirrors were placed along the entire length of the device, with length chosen to maintain a constant $\lambda^*/\ell_c = .25$ in each mirror cell. The energy flows between the hot and warm components and the thermal converter are shown in Fig. 15. The hot component is nonmaxwellian with density $n_h$, and is supplied by an energetic neutral deuterium beam with beam energy $E_o$. The warm component is Maxwellian at temperature T, consisting of a density $n_d$ of deuterium and $n_t$ of tritium. The total ion density $n_i = n_h + n_d + n_t$. As shown in Fig. 15, of the injected beam power density $P_b$, a power density $P_t$ is collisionally transferred to the warm component, with a small scattering loss $P_s$ remaining. Fusion reactions between both hot and warm deuterons, and warm tritons, produce neutron power densities $p_{nh}$, $P_{nw}$ and alpha particle power densities $P_{\alpha h}$, $P_{\alpha w}$, respectively. The alpha particles deposit their entire energy in the warm plasma.

The velocity distribution of the hot component is obtained from the Fokker-Planck Equation,[11] or by using an average energy approach.[31] The power densities $P_s$, $P_t$, $P_{nh}$ and $P_{\alpha h}$ are then evaluated. These power densities, along with $P_{nw}$, $P_{\alpha w}$ and $P_\beta$ all scale proportional to $n_e^2$, independent of the reactor length L. On the other hand, the multiple mirror

loss $P_\ell$ is proportional to $T^{7/2}/L^2$, independent of $n_e$. The equation for power balance in the warm plasma can be cast in the form

$$\frac{1}{p_1^2 L^2} = X(E_o, T, f, \varepsilon, M_1)$$

where $f = n_d/(n_d+n_t)$, $\varepsilon = n_h/n_e$, $M_1$ is the mirror ratio, and the plasma pressure $p_1 \propto n_e$ has been used. Thus, if the plasma pressure is doubled, the reactor length is halved. The subscript 1 refers to quantities evaluated in the center cell.

To optimize the system, we write $Q(E_o, T, f, \varepsilon, M_1) = P_f/P_b$, where $P_f$ is the total thermal fusion power density. Holding Q fixed, we maximize X. For a given $M_1$, optimum values of $E_o$, T, f and $\varepsilon$ are then determined. For these values, a minimum reactor length is found.

A neutral beam driven, multiple mirror reactor may be operated in two possible modes. For Q less than about 3.0, a pure two component mode ("wetwood burner") produces the smallest reactor length. The warm plasma is pure tritium ($f = 0$), and all fusion reactions arise from the interactions of beam deuterons with warm tritons. For Q greater than 3.0, the minimum length system has a warm component containing both tritons and deuterons $f > 0$, with $f \to 0.5$ as Q tends toward the self-sustaining condition $Q \to \infty$. Fusion reactions between deuterons and tritons in the warm plasma play an important role, and dominate the behavior as $Q \to \infty$.

## B. *Wetwood Burner Reference Reactor Design*

A Q of 2.1 has been chosen for the reference reactor design, corresponding to a wetwood burner mode of operation. For this reactor,

the energy confinement time for the pure triutium, warm component $\tau_E$ is of the order of or shorter than the triton-electron energy exchange time $\tau_{ie}$. This allows the warm-ion temperature $T_i$ to be significantly depressed below the electron temperature $T_e$. Since the axial power loss scales as $T_i^{5/2}(T_i+T_e)$, the axial energy loss is reduced, while the hot component fusion reactions are maintained.

The power balance equations for the warm electrons and the tritons have been solved self-consistently, assuming unequal electron and ion temperatures.[34] For the beam and $\alpha$ particles, average powers have been used, rather than those calculated from the Fokker-Planck Equation. For given values of the beam energy $E_o$, $T_e$ and $T_i$, the relative beam density $\varepsilon$, the reactor Q, and the product $p_1 L M_1$ have been determined. The value of $p_1 L M_1$ has been minimized with respect to $E_o$, $T_e$ and $T_i$. The results are presented as a graph of $p_1 L M_1$ vs reactor Q, as shown by the steep solid curve in Fig. 16. At $Q = 1.5$, the reactor length is reduced by almost a factor of two, as compared with the equal temperature case. For $Q = 2.5$, the length reduction is about 30%.

Choosing representative values of $\eta_{DC} = 0.8$ and $\eta_T = 0.5$, we find for $Q = 2.1$ that $Q_E = 2$, a reasonable value on economic grounds. Reasonable choices for the plasma $\beta$ and the mirror ratio are $\beta = 0.8$ and $M_1 = 3.3$. We then find $E_o = 180$ keV, $T_e = 6$ keV, $T_i = 4.5$ keV, $p_1 = 290$ bar, $\varepsilon = .16$, $n_1 = 7.7 \times 10^{15}$ cm$^3$, $\lambda_1 = 25$ m, and $\tau_E = 0.6$ msec. The reactor consists of 7 cells and is 320 meters long, with a midplane (vacuum) field B of 9.3 T and a mirror (vaccum) field $B_{1m} = 14$ T. For $P_{net\ electrical} = 1500$ MW, the plasma diameter in the center cell $d_1$ is 3.0 cm, the mean plasma

diameter, averaged over z, is 6 cm, and the injected beam current is 8.3 kA.

The min-ave-B magnetic fields can be generated entirely by superconducting coils placed outside the reactor blanket in the usual manner. Alternatively, the solenoidal and weak quadrupole fields can be generated using superconducting coils, with required mirror-strong quadrupole fields near the mirror throats being generated by small, "baseball-type" copper coils placed inside the blanket. In this case, the copper coils must generate a field of $B_{1m}-B_1 = 4.7$ T. The ohmic power dissipation in such coils can be a small fraction of the total output power of the reactor, as described in Section V-G.

The maximum cross-sectional area available for neutral beam injection is $L\bar{d}$, where $\bar{d}$ is the average plasma diameter. For injection along a single diameter, this implies an average beam current density of 0.43 kA/m$^2$. For a beam source currently being developed of 10 kA/m$^2$, four percent of the reactor length would be used for injection. This requires aproximately 30 beam sources at this density of the type now being designed at the Lawrence Berkeley Laboratory.[33] The varying plasma density along the reactor length allows matching of the neutral beam energy absorption to the plasma line density across a diameter. The subsequent energy transfer, primarily to the electrostatically confined electrons, is distributed axially throughout the plasma.

The theory of neutral beam ionization has been worked out in considerable detail.[34] For our purposes we have used these results to calculate the beam attenuation in the form

$$I = I_o \exp \left[ -n \langle \sigma v \rangle_{tot} \, r/v_b \right]$$

where $\langle \sigma v \rangle_{tot}$, the reaction rate for ionization is a weak function of the beam energy and plasma parameters, $v_b$ is the beam velocity, n the plasma density, and r the attenuation distance. For the wetwood burner operation, the design case of $E_b = 180$ keV and the typical plasma parameters, we find $v_b/\langle \sigma v \rangle_{tot} = 5 \times 10^{15}$ cm$^{-1}$. To obtain an attenuation by $1/e^2$ to the center of plasma ($r = 1.5$ cm) we find $n = 6.7 \times 10^{15}$ cm$^{-3}$. This implies injection into an axial density slightly lower than the peak axial density of $n_1 = 7.7 \times 10^{15}$ cm$^{-3}$. For the higher density operation with interacting D-T lower energy ion species, a combination of higher beam energy and operation further down the axial density distribution would be required.

Start-up does not appear to be a problem in a multiple mirror reactor. If the plasma density is maintained at its reactor value, beam trapping efficiency is essentially constant down to arbitrarily low plasma energies. The rate of energy transfer to the plasma increases with decreasing plasma temperature. Energy loss from the plasma decreases at least as fast as $1/T^{3/2}$, and is negligible at low plasma energies. Thus, build-up of plasma energy proceeds rapidly toward the operating temperature. An additional requirement both for stability of operation and build-up is that at the operating temperature $dP_{net}/dT < 0$, which implies that T be chosen slightly higher than the temperature which maximized Eq. (14). This requires slightly more beam power if all other parameters are held constant.

In making the above choice of reactor parameters, we have opted for a high but practical magnetic field strength, in order to minimize the device length. If these requirements ($B_{1m} = 14$ T) are difficult to achieve in an average minimum B field configuration, they may be relaxed at the expense of an increased reactor length. For example, consider doubling the length from 320 m to 640 m. For constant Q, $M_1$, and $\beta$ the the multiple mirror scales as $B^2L = \text{constant}$, such that all magnetic fields are reduced by .707 of their original value. The superconducting solenoidal field is then 6.6 T and the additional normal mirror field is 3.4 T. These values appear to be obtainable even with today's technology. $I^2R$ losses and forces in the mirror-quadrupole coils have both been reduced by a factor of 2. To keep the same number of Larmor radii across the device we hold $rB = \text{constant}$, implying an increase in radius by a factor of $\sqrt{2}$. The total fusion power is proportional to $n^2r^2L$, and is thus constant. Since Q is also constant, the beam power is constant, but can be spread over a larger area. The new area $L\bar{d}$ is 2.8 times larger, implying at 10 $kA/m^2$ current density, that roughly 1.6% of the reactor length is used for beam injection. Holding the wall loading constant keeps the power density within the vacuum chamber constant, but lowers the power density, within the magnetic field structure by about $\sqrt{2}$. The result is a redesigned lower field reactor which has nearly the same characteristics as the higher field one, except for length.

### C. *Conventional Beam-Driven Reactor*

For $Q \geq 3$, the optimum reactor mode of operation consists of a warm plasma containing both tritons and deuterons. Both beam-triton and

warm-component DT fusion reactions occur, although typically the latter dominate. The energy confinement time $\tau_E$ is longer than the ion-electron equilibration time, so that the equal temperature assumption $T_i = T_e$ is valid. The power balance equation has been solved in this limit.[11] The solid curve to the right in Fig. 16 shows $p_1 LM_1$ plotted against the reactor Q. For comparison, the dashed curve shows $p_1 LM_1$ for a conventional mutliple mirror reactor driven by some means other than neutral beam injection, such that beam-triton fusion reactions are absent.

For comparison with the more favorable wetwood burner mode of operation, we again choose to examine the case $Q = 2.1$, $\eta_{DC} = 0.8$, $\eta_T = 0.5$, $Q_E = 2$, $\beta = 0.8$ and $M_1 = 3.3$. At this Q, $T = 4.8$ keV, $E_o = 180$ keV, $f = .28$ and $\varepsilon = .002$. For a reactor length of 320 m, we then have $p_1 = 900$ bar, $n_1 = 6.4 \times 10^{16}$ cm$^{-3}$, mean free path $\lambda_1 = 3.1$ m, center cell length $\ell_{c1} = 3.7$ m, and end cell length $\ell_{ce} = 24.3$ m. The reactor consists of 30 (variable length) cells, and the energy confinement time is $\tau_E = 2.9$ ms. We also have $B_1 = 16.5$ T (superconducting solenoidal field) and $B_{1m} = 25$ T (8.5 T additional normal field coil). For the reactor to generate $P_{net} = 1500$ MWe, we have an injected neutral beam current $I_b = 8.3$ kA and a center cell plasma diameter $d_1$ of 3.6 cm. The magnetic field requirments are severe, but they can be scaled down by increasing the length, as noted in the previous section. Doubling the length to 640 m, for example, reduces the field by $1/\sqrt{2}$ to 11.7 T in the superconducting solenoid and 6 T additional normal field in the mirrors.

## D. Low Z Impurities

Another study involves the addition of a small fraction $f_z$ of a fully ionized, low Z impurity to the warm plasma.[11] This impurity produces effects in the power balance equation which are proportional to $Z^2 f_z$, $Z f_z$ and $f_z$. In addition, there are power flows due to free-bound and bound-bound bremsstrahlung if the impurities are not fully ionized. The dominant effects are those which scale as $Z^2 f_z$. These include (1) an increase in free-free bremsstrahlung radiation $P_\beta$, (2) a reduction in multiple mirror power loss $P_\ell$, due to increased scattering of warm D and T ions against the impurity ions. If the reduction in $P_\ell$ is greater than the increase in $P_\beta$ and $P_s$, then the addition of impurities may actually enhance confinement, i.e., cause the reactor length to decrease.

A code has been developed to minimize the system length, including all these terms. A corona equilibrium model was used to estimate the fractional impurity ionization. Typical results for a high impurity concentration, $\sim$1%, are shown in Fig. 17. It can be seen that there is a reduction in system length of order 10%. Reactor operation is insensitive to impurities, which may even be beneficial. Also of significance, multiple mirror operation is possible at considerably higher temperatures than in the absence of impurities. This is of importance because in the absence of impurities E and T ions in the extreme Maxwellian tail of the warm component generate the bulk of the fusion power.

At these high impurity concentrations (of order 1%), there will be significant radial loss of warm ions due to classical diffusion against these impurities. This effect has not been studied in detail. However,

a crude estimate suggests a factor of ten enhancement, which implies radial loss roughly half the axial loss for the reference reactor design radius. For impurity concentrations considerably less than 1% the enhanced radial losses are not significant.

### E. *Other Energy Losses*

Other energy loss processes, which have been neglected in the foregoing analyses, include synchrotron radiation, radial diffusion, and axial and radial heat flow. Synchrotron radiation losses are negligible for these low temperature, high density regimes.

As discussed in Section II-B, for the design reactor, like particle diffusion is more than a factor of 10 slower than axial diffusion. Classical diffusion is also negligible for the parameters considered here. This is seen by comparing the radial diffusion time

$$\tau_r = \frac{(M/m)^{\frac{1}{2}} R^2 \lambda}{a_i^2 v_i}$$

to a typical energy confinement time $\tau_E$. For typical multiple mirror parameters, $a_i/r_p \approx 0.2$ and $\lambda/v_i \approx 10^{-5}$ sec, yielding $\tau_R \approx 25$ msec, more than an order of magnitude larger than the energy confinement time $\tau_E \approx 0.6$ msec. The plasma column is assumed to be isolated from the chamber wall by a vacuum layer. This layer is maintained even in the presence of radial diffusion, since enhanced confinement due to multiple mirror action ceases at the low density plasma edge. The edge particles are therefore lost axially, rather than flowing radially to the wall. The radial

temperature distribution is thus assumed to be uniform, and energy loss due to radial heat flow is negligible.

If the confining magnetic field is not axisymmetric, then radial losses will be enhanced. In particular, if minimum average B fields are used, enhanced radial losses will occur near the fanshaped flux surfaces at the mirror throats, as discussed in Section II-B. A calculation of radial diffusion in elliptical geometry, including the effects of both ion-electron and ion-ion collisions, indicated a considerable parameters range over which radial losses, while enhanced, are still small compared to multiple mirror axial losses.[15]

As pointed out previously, electron heat flow and the resulting cooling of ions on electrons must be prevented by separating the plasma from the end wall with an insulating sheath. In one possible end configuration,[25] a distributed sheath is generated by expanding the end loss plasma, reducing both the number and the power density of the plasma to some reasonable value near the end wall. It has been estimated[35] that the insulating sheath will be maintained provided that the power is kept below 200 $W/cm^2$, to prevent the emission of cold electrons from the end wall. For a 1500 MW end loss this requires 750 $m^2$ of collector area, divided equally between the two ends.

In the preliminary feasibility calculation, it was assumed that every ion lost an average energy 3T axially, and that an electron with equal average energy was also lost. The axial energy loss per ion-electron pair was thus taken to be of order 6 T. However, the existence of an insulating sheath of order 4 T results in the loss of an ion with average thermal energy of order 3 T and directed energy of order 4 T, accompanied

by an electron with energy of order T. The total axial energy loss per ion per electron pair is then of order 8 T, rather than 6 T, leading to an increase in reactor length by a factor of $(4/3)^{\frac{1}{2}} = 1.15$. However, this increase can be compensated by a small increase in the direct conversion efficiency, an increase which seems reasonable in view of the directed nature of the ion energy spectrum when it is accelerated through a 4 T sheath potential.

The axial electron heat flow time within the confined plasm is short, of order $L^2/\lambda v_e \approx 10^{-4}$ sec. Thus, the electron temperature within the plasma is a constant, independent of axial position z. Axial ion heat flow within the confined plasma tends to maintain the ion temperature constant with z. Axial ion heat flow across the insulating sheath does not occur, since the ions are in a low density, collisionless regime in this region. However, the basic multiple mirror loss rate is enhanced by the ambipolar potential in the plasma. The enhanced loss rate has been used in the feasibility calculations.

## F. *Nonclassical Collisions*

With the mean free path dependent on classical interparticle collisions, the range of densities for which favorable scaling occurs is limited and a reactor requires high magnetic fields and long lengths. If a scattering mechanism exists independently of collisions between particles, then reactor parameters can be found with considerably lower field and length requirements.

A preliminary evaluation of the collision - independent multiple mirror concept as a steady-state reactor has been made[12] by estimating

the parameters for a self-sustaining reactor independently of the physical mechanism of producing diffusive loss. We assume a reactor with constant temperature T, linear density profile, and constant cell length $\ell_c$ and mirror ratio M. We assume that a process exists for limiting the mean free path to a cell length, and the effective time between steps, to the transit time multipled by the ratio of trapped-to-untrapped phase space. The axial power loss per unit volume is then calculated to be

$$P_\ell = \frac{32 p_1 \ell_c v_T}{2\pi L^2 M} \tag{15}$$

where $v_T = (kT/m_i)^{\frac{1}{2}}$, $p_1 = 2n_1 kT$ is the plasma pressure, and the power loss includes the usual enhancement due to electron energy loss and ambipolar effects. The self-sustaining reactor condition $P_\alpha = P_\ell + P_\beta$ yields

$$\frac{\ell_c}{L^2 p_1 M} = H(T) \ . \tag{16}$$

H(T) has a maximum $H_{14}$ at $T \approx 14$ keV. We then have

$$L = \left( \frac{\ell_c}{p_1 M H_{14}} \right)^{\frac{1}{2}} \tag{17}$$

independent of the process producing the diffusion.

For a given maximum pressure $p_1$, there are three factors which act to reduce L below the collisional multiple mirror reactor length $L_{col}$, as follows:

(1) The cell length $\ell_c$ can be smaller than the optimum cell length for the collisional multiple mirror confinement.

(2) The optimum plasma temperature of 14 keV is larger than the optimum for collisional multiple mirror confinement (6 - 7 keV) thus leading to a larger value of H.

(3) The effective mirror ratio M can be much larger than for collisional multiple mirror confinement.

The total reactor fusion power is given by

$$P_f = .034\, A p_1^{3/2} \left(\frac{\ell_c}{M}\right)^{\frac{1}{2}} \tag{18}$$

where $P_f$ is in MW, $p_1$ in bars, the reactor cross-sectional area $A = \pi r_p^2$ is in $cm^2$, and $\ell_c$ is in m.

The value of $\ell_c$ and R are determined by the particular noncollisional confinement scheme which is employed. As an example, we choose $\ell_c/M = 0.1$ m. With these assumed conditions, self-sustaining reactor lengths are modest. For example, at a pressure $p_1$ of 400 bar and a fusion power $P_f = 3000$ MWt, the reactor length is 225 m and the central plasma diameter is 6.6 cm. These results are considerably more favorable than those obtained for collisional scattering where a self-sustaining length of 2200 m was calculated at a pressure of 1200 bar.

Possible methods of decoupling pitch-angle scattering from interparticle collisions are by introducing nonadiabatic effects, either with low field regions, or with rapidly varying fields. These effective collisions, induced by the breaking of magnetic moment invariance in low field midplane regions of a multiple mirror system, are currently under study. The collisions can lead to enhanced radial loss; however, as noted in Section II-B, enhanced radial loss does not occur in an axisymmetric system

due to the invariance of the canonical angular momentum $p_\theta$. Numerical studies of radial diffusion in such systems are currently being performed, using the TIBRO code.

## G. *Reactor Design*

Little attention has been given to the design of specific reactor components. The axially averaged neutron power loading is of order 10 MW per meter of length, with the bremsstrahlung power loading being perhaps 1/10 of that. The wall loading is adjusted by varying the wall diameter. For a neutron loading of 3 $MW/m^2$, the diameter is 1 m.

For the wetwood burner reference reactor design of Section V-B, with a reactor length of 320 m, the coil system consists of a linear superconducting solenoid plus weak quadrupole coil generating a field of 9.3 T, with mirror and strong quadrupole fields provided by either superconducting coils, or by small, steady state nonsuperconducting coils which add 4.7 T to the superconducting solenoidal field. No studies of superconducting magnet design have been made. The design of a nonsuperconducting simple mirror coil to generate 10 T fields has been examined in order to identify problems and difficult design constraints. The coil design finally considered was of hard drawn copper, water cooled, Bitter design ($j \propto r^{-1}$). Higher strength copper alloys might also be used. The inner diameter was 10 cm, the outer diameter was 40 cm, and the coil length was 20 cm. The coil is placed inside the neutron blanket. The following factors were considered in the design: (1) magnetic forces and mechanical stress, (2) ohmic power dissipation, (3) neutron energy deposition, (4) bremsstrahlung energy deposition, (5) cooling requirements, (6) neutron damage and (7) activation. The most critical factors

were (1) and (2), both of which biased the design toward small dimensions. The ohmic power dissipated in a single coil is about 2 MW. For the wet-wood burner reactor design, the ohmic power loss for eight coils is then of order 16 MW, for a 1500 MWe net power output reactor.

Little consideration has yet been given to the design of coils producing min-ave-B fields. It is expected that the solendoidal field, and the weak quadrupolar field in the cell midplanes, will be generated using, respectively, a superconducting solenoid and a set of superconducting, linked quadrupole bars. The mirror fields and the strong quadrupolar fields near the mirror throats may be geneated by either superconducting or by conventional coils. Difficult constraints are imposed on the design of these coils. The coil structure must support the high stresses and generate the spatially varying fields requred by the min-ave-B condition. For a realization using conventional coils, the use of separate Bitter-type magnets to generate both mirror throat, leads to considerable ohmic power dissipation. The evaluation of a "Baseball" coil design is a logical next step in examining the feasibility of magnet design for achieving min-ave-B in a reactor. This evaluation is currently under way. An alternate concept is the fitting of current elements to the current patterns on an elliptical flux surface near the fans.

## REFERENCES


1. B. G. Logan, A. J. Lichtenberg, M. A. Lieberman and A. Makhijani, Phys. Rev. Lett. 28 144 (1972).
2. J. B. Taylor, "Multiple Mirrors and R. F. Stoppers," in Culham Laboratory Report CLM-R94, p 27, U.K.A.E.A., England (1969).
3. G. I. Budker, V. V. Mirnov and D. D. Ryutov, ZHETF Pis. Red. 14, 320 (1971).
4. V. V. Mirnov and D. D. Ryutov, Nuclear Fusion 12, 627 (1972).
5. B. G. Logan, I. G. Brown, M. A. Lieberman, and A. J. Lichtenberg, Phys. Rev. Lett. 29, 1439 (1972).
6. A. Makhijani, A. J. Lichtenberg, M. A. Lieberman, B. Grant Logan, Phys. of Fluids 17, 1291 (1974).
7. B. G. Logan, I. G. Brown, M. A. Lieberman, and A. J. Lichtenberg, Phys. of Fluids 17, 1302 (1974).
8. G. I. Budker, V. V. Danilov, E. P. Kruglyakov, D. D. Ryutov, and Ye. V. Shun'ko, "Experiments in Confining a Plasma in a Multi-mirror Magnetic Trap," MATT-Trans 108, Princeton Plasma Phys. Lab. (1973).
9. G. I. Budker, "Thermonuclear Fusion in Installations with a Dense Plasma," 6th Eur. Conf. on Plasma Phys. and Contr. Nuclear Fusion.
10. H. L. Berk, "Flow in a Multiple Mirror", unpublished.
11. S. T. Yang and M. A. Lieberman, "Power Balance and Impurities in Two-Component, Multiple Mirror Reactors," Nucl. Fusion 17, 697 (1977).
12. A. J. Lichtenberg and M. A. Lieberman, Nuclear Fusion 16, 533 (1976).
13. J. L. Tuck, Phys. Rev. Lett. 20, 715 (1968).
14. H. P. Furth, J. Killeen, M. N. Rosenbluth, and B. Copi, Proc. Culham Conf. on Plasma Phys. and Contr. Nucl. Fusion Res. 1, p 103 (1965).

15. M. Tuszewski and A. J. Lichtenberg, "Two-Dimensional Boundary Value Problem for Ion-Ion Diffusion," Phys. of Fluids 20, 1263 (1977).

16. M. Tuszewski, A. J. Lichtenberg and S. Eylon, "Transient Confinement of High Density Plasma in a Multiple Mirror," Nucl. Fusion (to be published).

17. L. C. Steinhauer, Phys. of Fluids 19, 738 (1976).

18. H. P. Furth and M. N. Rosenbluth, Phys. of Fluids 7, 764 (1964).

19. J. C. Riordan, "Stabilization of Interchange Modes in Multiple-Mirror Plasmas, Ph.D. Thesis, University of California, Berkeley (1976).

20. M. A. Lieberman and S. L. Wong, "Axial Feedback Stabilization of Flute Mode in Mirror Reactor," Plasma Phys. 19, 745 (1977).

21. B. Grant Logan, "Current-Stabilization of the Curvature Driven M = 1 Mode," Lawrence Livermore Laboratory Report UCID 16615 (1974).

22. R. W. Moir, Ed., Committee Report: Lawrence Livermore Laboratory Re-Evaluation of the Simple Mirror for a Fusion Reactor, App. D, UCID-16736 (1975).

23. J. C. Riordan, M. Tuszewski, and A. J. Lichtenberg, "Stabilization of Interchange Modes in Multiple-Mirror Confined Plasma," Plasma Phys. (to be published).

24. J. C. Riordan and C. Hartman, "Interchange Instability with Line-Tying and Finite Larmor Radius Effects," Phys. Fluids 20, 1376 (1977).

25. R. W. Moir and W. L. Barr, Nucl. Fusion 13, 35 (1973).

26. A. Boozer, private communication (1976).

27. A. J. Lichtenberg and B. R. Myers, Bull. Am. Phys. Soc. 17, 1058 (1972).

28. J. Benford et al., "Electron Beam Heating of Linear Fusion Devices," presented at the First Inter. Topical Conf. on Electron Beam Res. and Tech., Albuquerque, N.M. (USA), November 3 - 5 (1975).

29. "The Electron Beam Heated Solenoid Reactor: A Proof-of-Principle Experiment," Vol. I, Physics International, San Leandro, Calif., December (1976).

30. F. L. Ribe, "Fusion Reactor Systems," Los Alamos Scientific Laboratory Report LA-UR-74-758.

31. S. T. Yang and M. A. Lieberman, "Two-Component, Multiple Mirror Reactor with Depressed Ion Temperature," Nucl. Fusion 18, 965 (1978).

32. S. L. Wong and M. A. Lieberman, "Axial Feedback Stabilization of Flute Mode in a Multiple Mirror" (to be published: Plasma Phys. (1978)).

33. W. B. Kunkel, Lawrence Berkeley Laboratory, private communication.

34. A. C. Riviere, "Penetration of Fast Hydrogen Atoms into a Fusion Reactor Plasma," Nucl. Fusion 11, 363 (1971).

35. R. W. Moir, Lawrence Livermore Laboratory, private communication (1977).

TABLE I

PARAMETERS OF the 10 METER MULTIPLE MIRROR EXPERIMENT

| | |
|---|---|
| $B_{max}$ = 20 kG | *maximum field in mirror throat* |
| M = 4 | *mirror ratio* |
| $\ell_m \approx$ R = 7.5 cm | *mirror scale length* |
| $\ell_c$ = 75 cm | *cell length* |
| N = 11 | *number of cells* |
| $r_p$ = 1.15 cm | *midplane radius for marginal stabilization* |
| Q = 23 | *fan ellipticity* |
| $r_{min}$ = .12 cm | *minor radius of fan* |
| $r_{max}$ = 2.8 cm | *major radius of fan* |
| $T_i \approx T_e$ = 10 - 50 | *volts* |
| $n_{max} = 10^{14} - 10^{15}$ | $cm^{-3}$ |

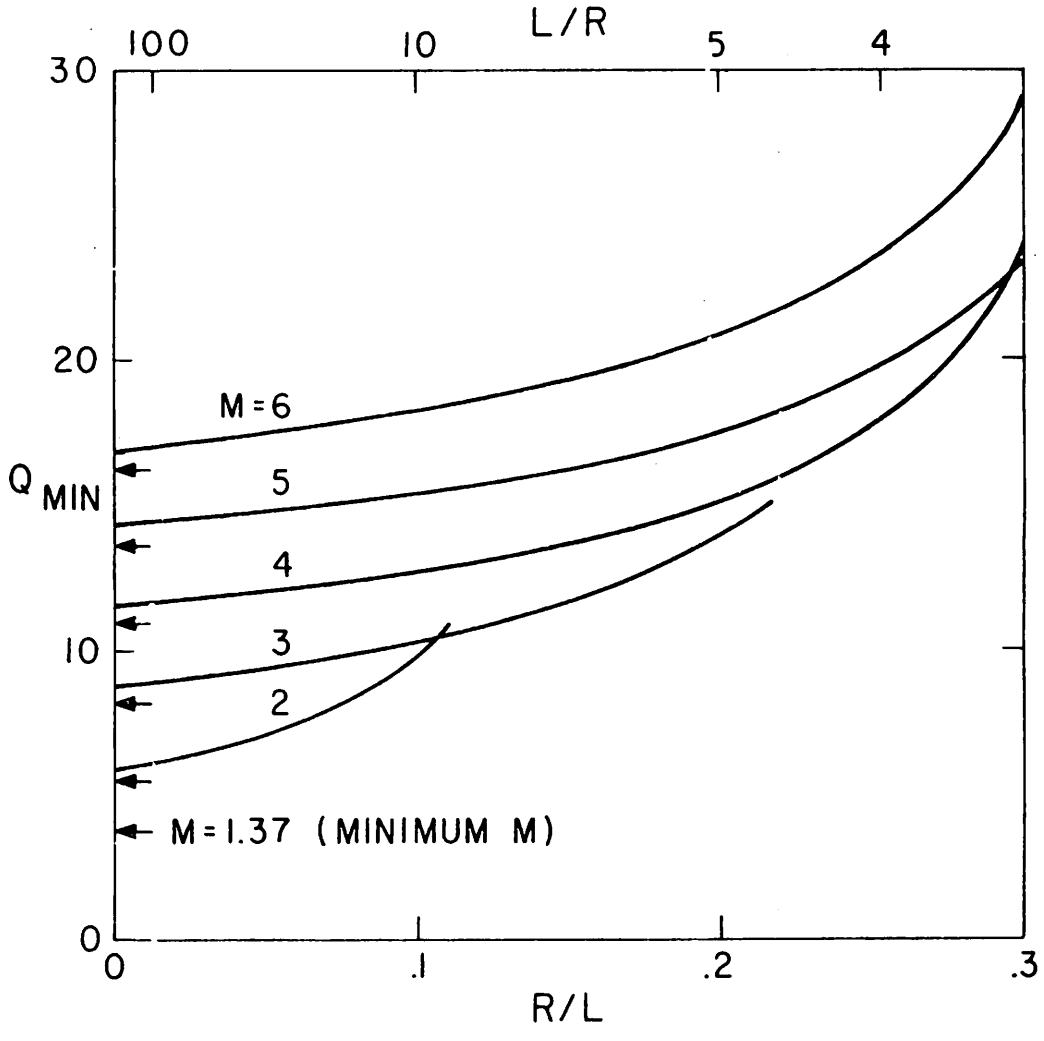


FIGURE 1 Minimum ellipticity $Q_{min}$ for marginal well; arrows indicate $Q_{min}$ for singular fields.

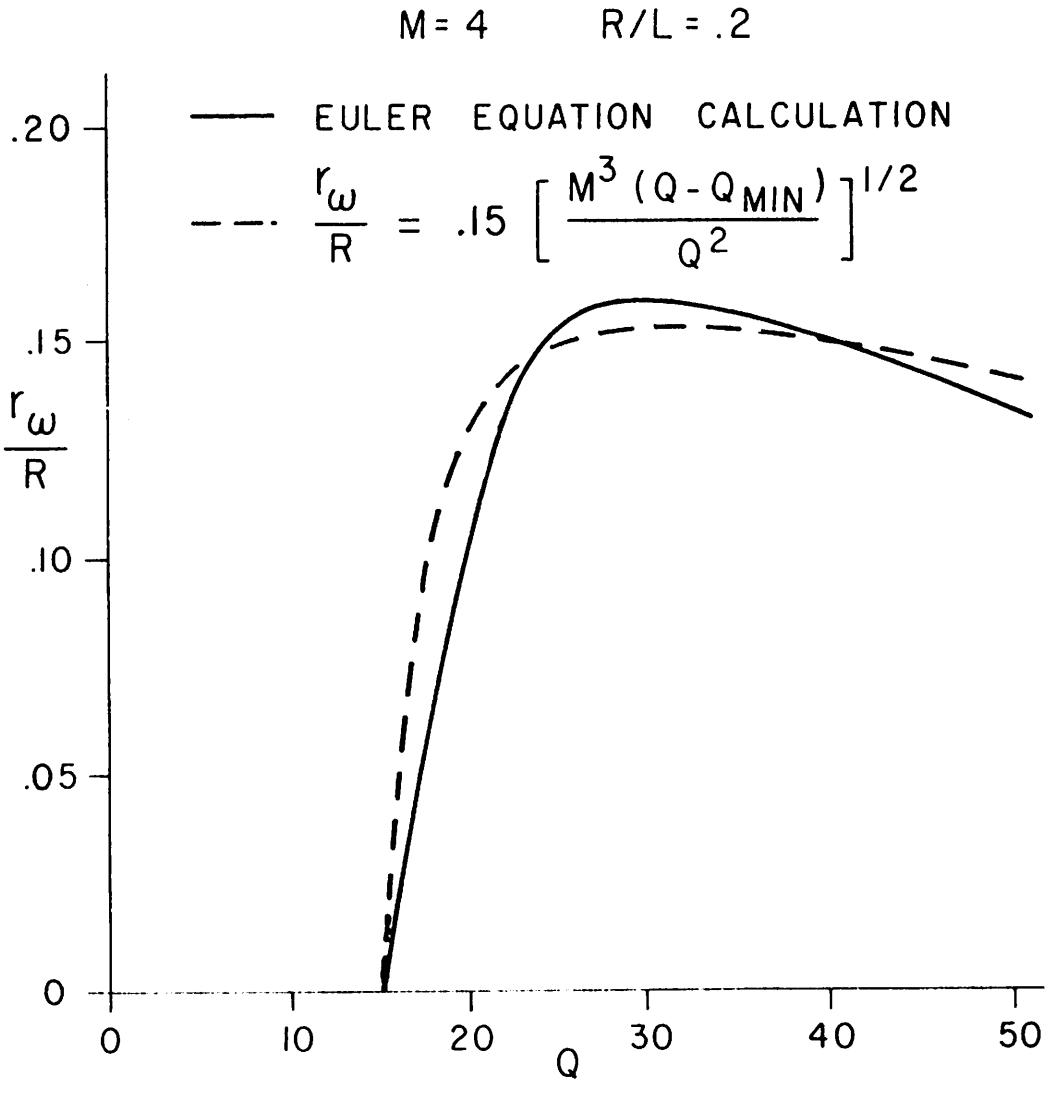


FIGURE 2 Well radius vs ellipticity.

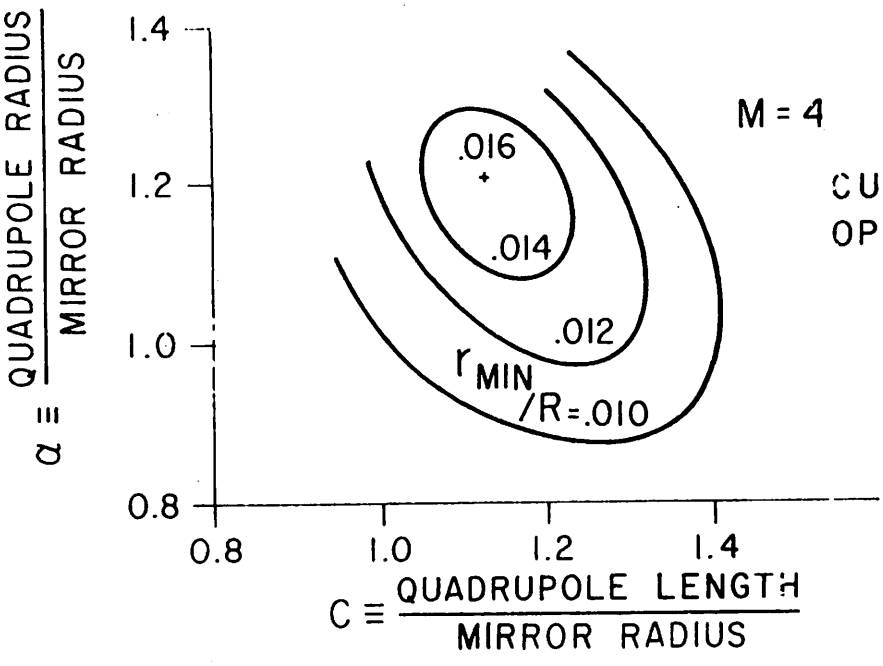


a) Maximized $r_{min}$ vs coil dimensions

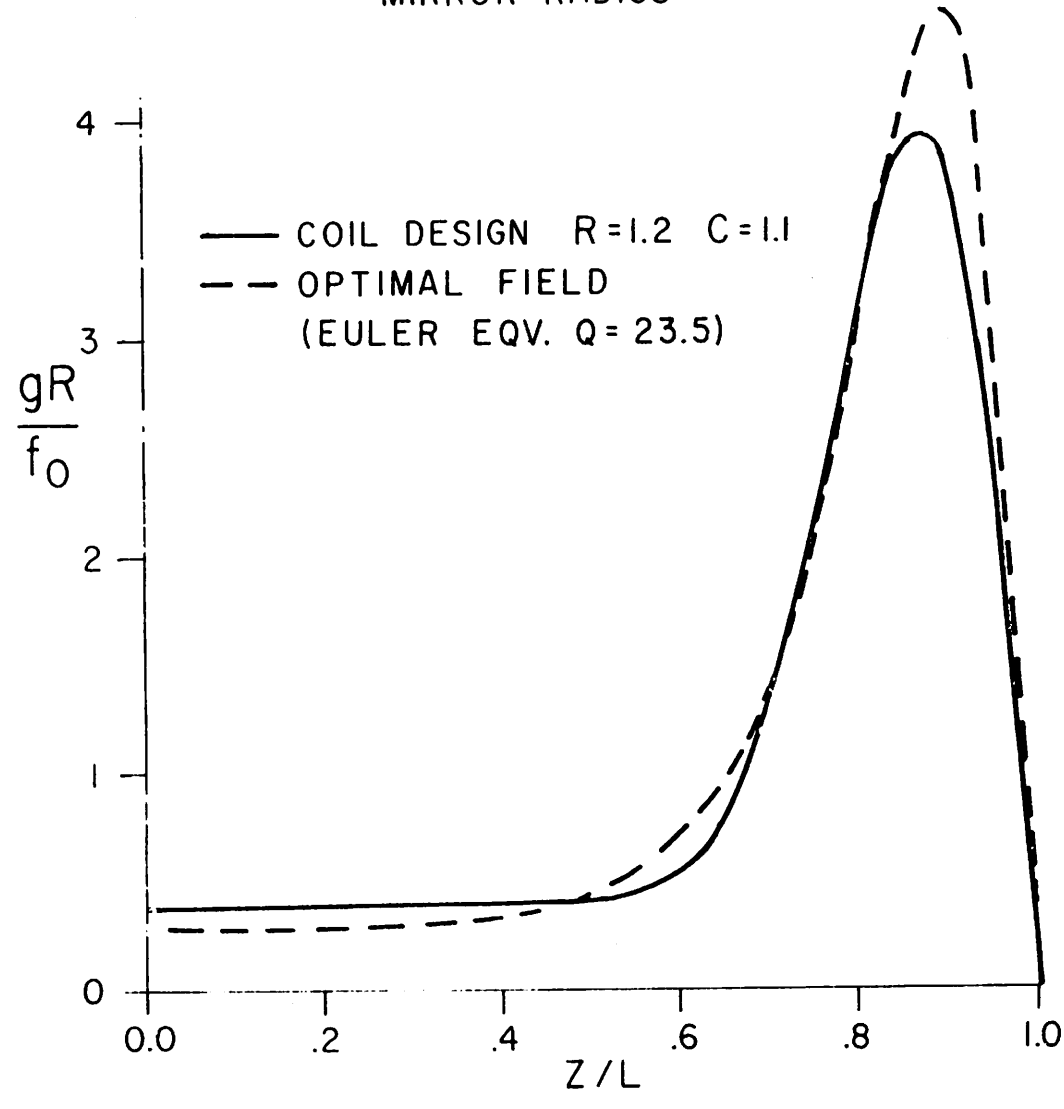


b) Comparison of quadrupole field shapes

FIGURE 3 Quadrupole field.

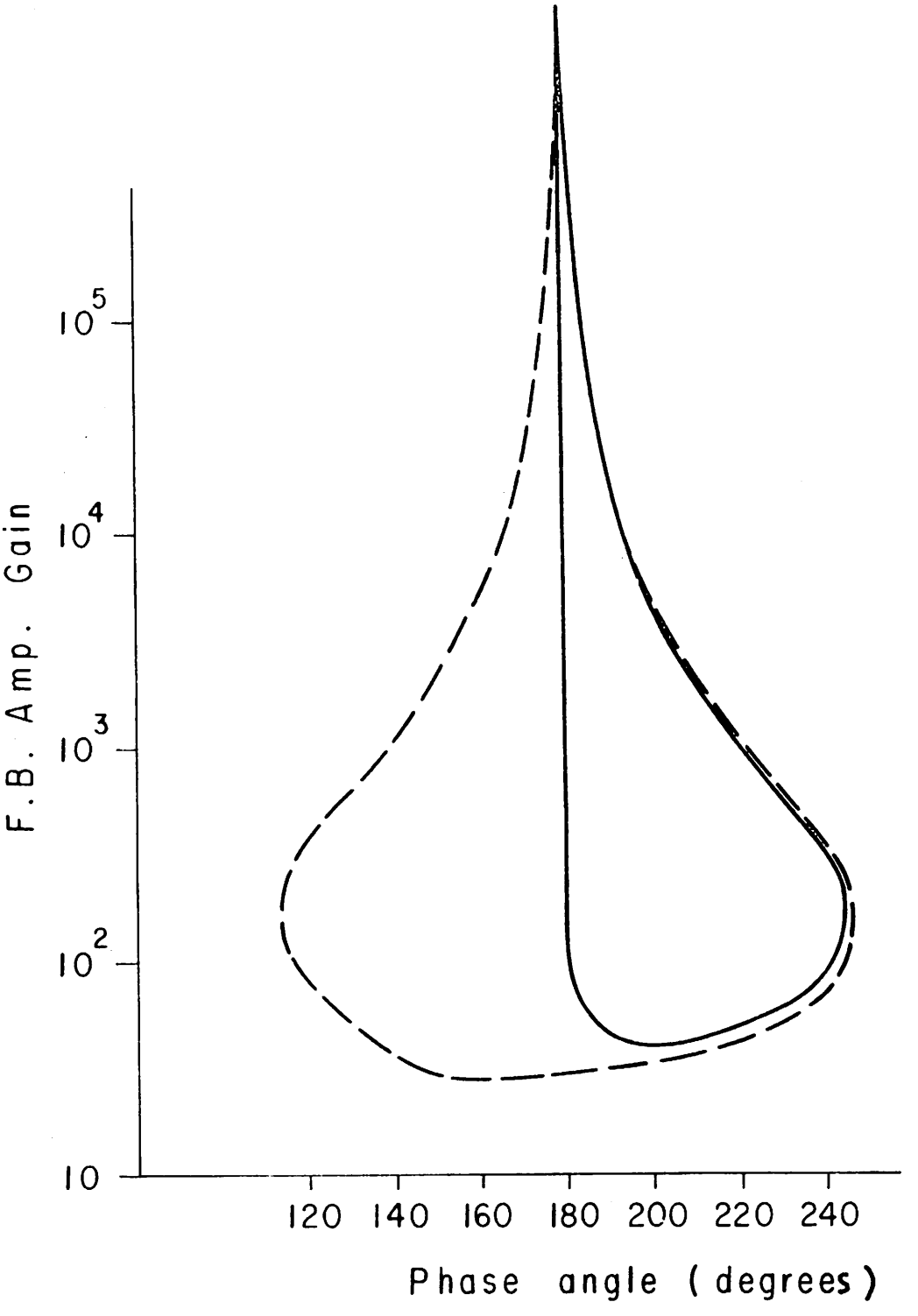


FIGURE 4 Feedback gain vs phase angle, showing theoretical stability boundaries for axial integral feedback stabilization. Solid curve: absolute stability. Dashed curve: unstable, with growth time greater than 400 μsec.

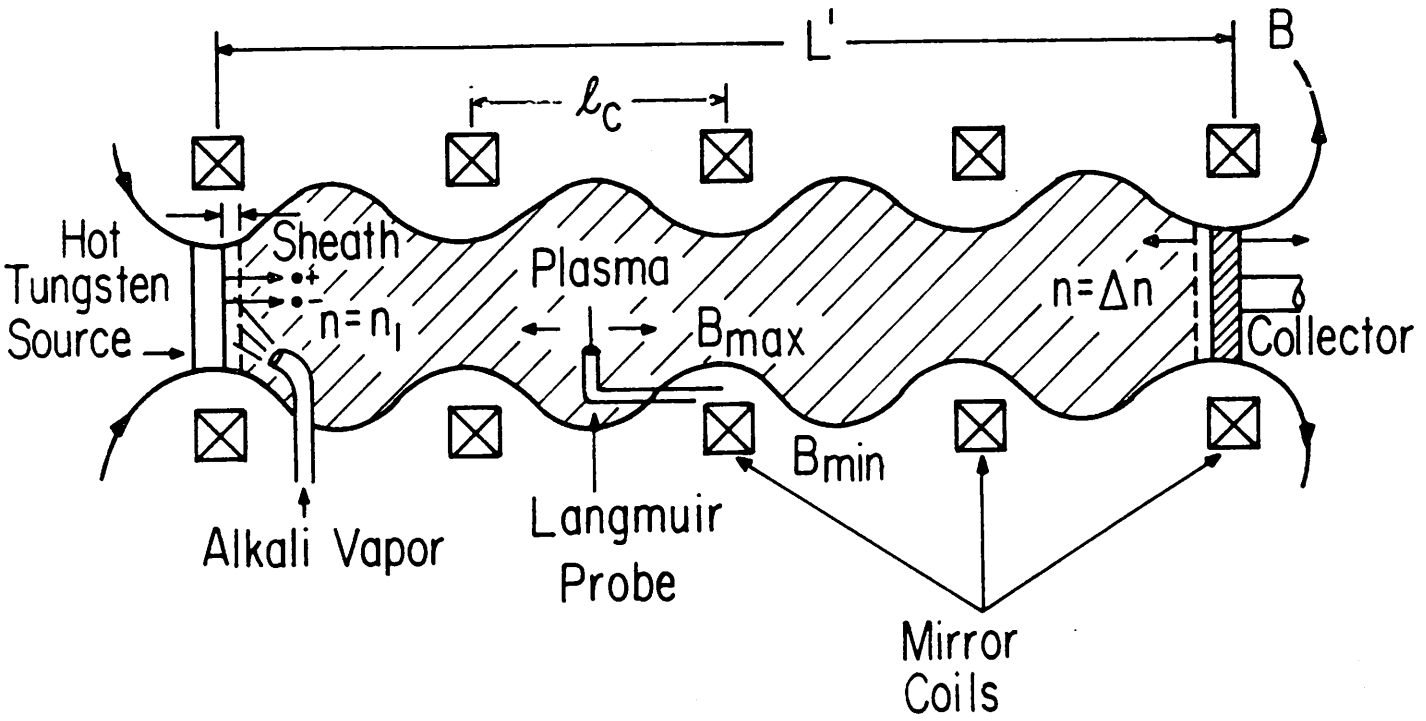


FIGURE 5 The multiple mirror experiment.

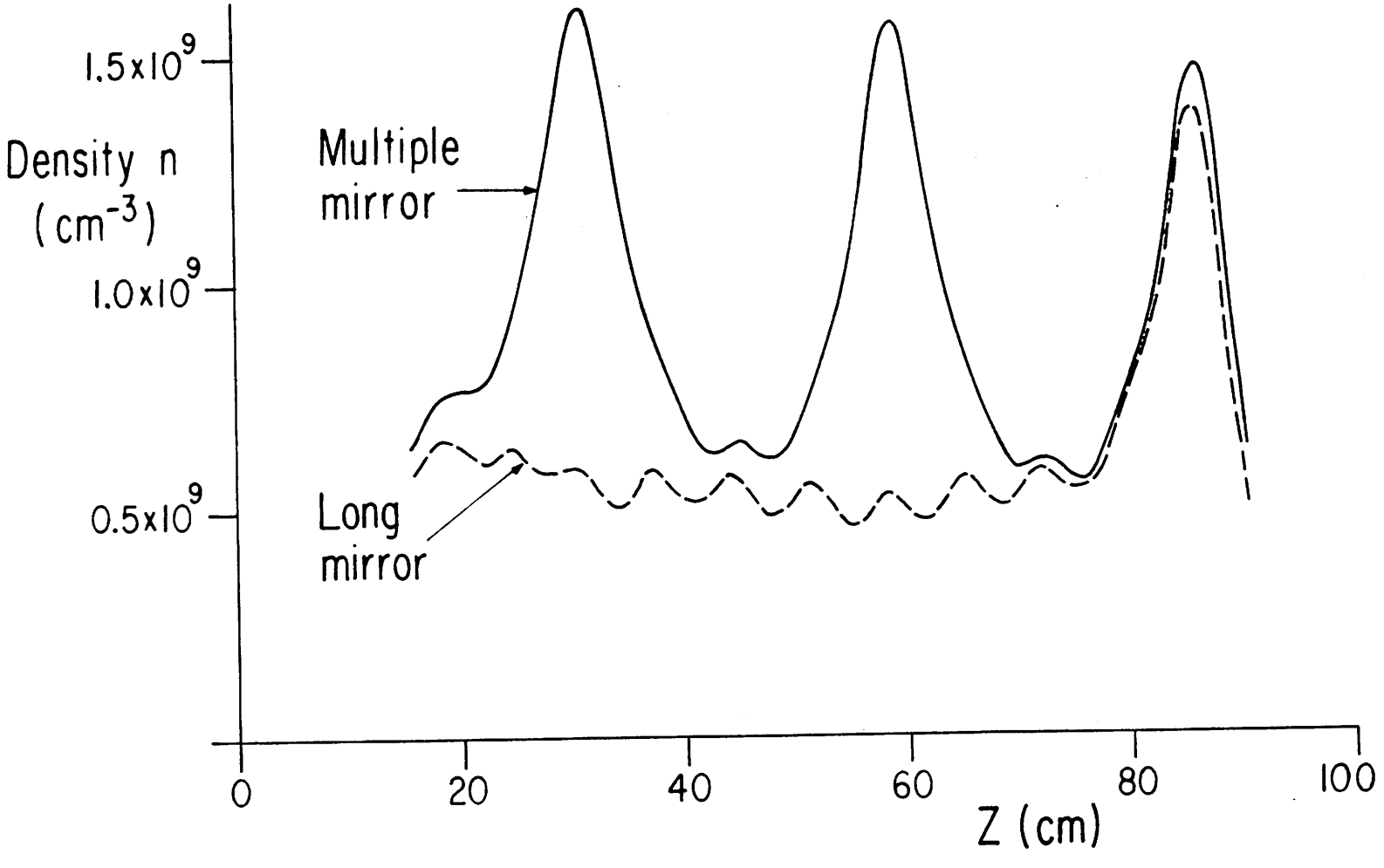


FIGURE 6a 3 cell (solid line) and long mirror (dashed line) density as a function of z for the low density regime. Potassium.

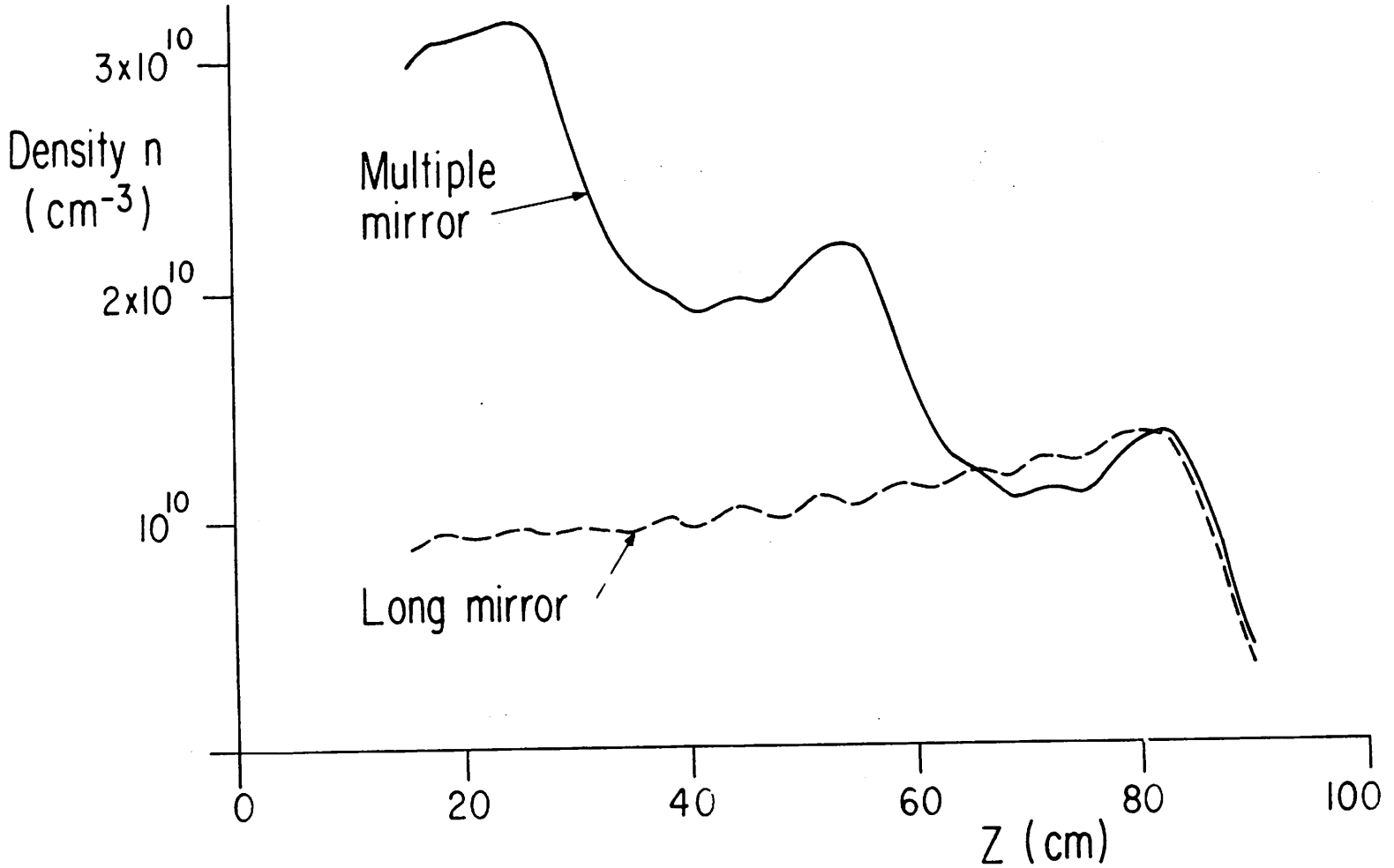


FIGURE 6b 3 cell (solid line) and long mirror (dashed line) density as a function of z for the intermediate density regime.

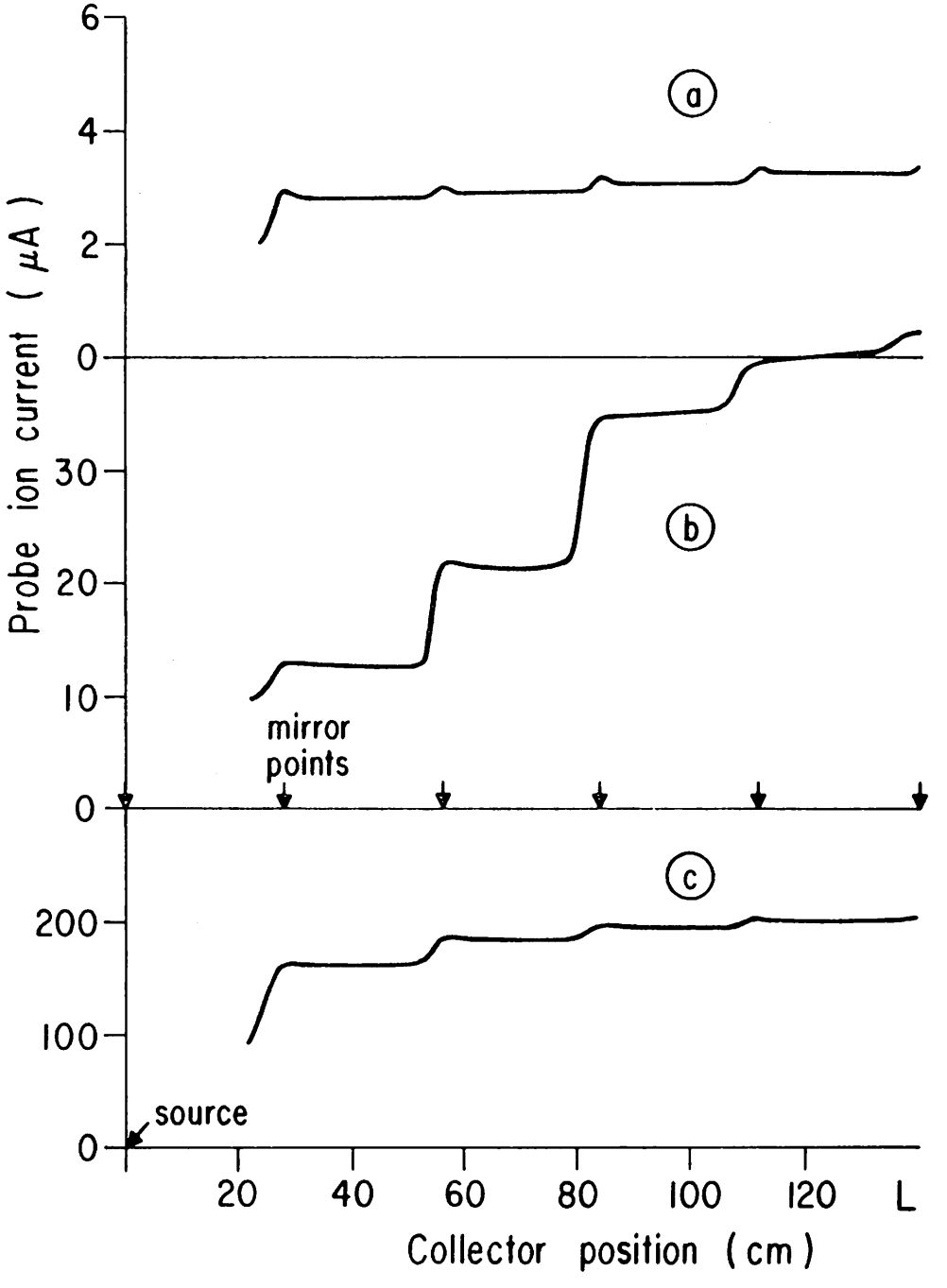


FIGURE 7 Langmuir probe ion saturation current (density $n_1$) in the first cell as a function of collector position, in the (a) low density, (b) intermediate density, and (c) high density regimes. Potassium, 5 cells.

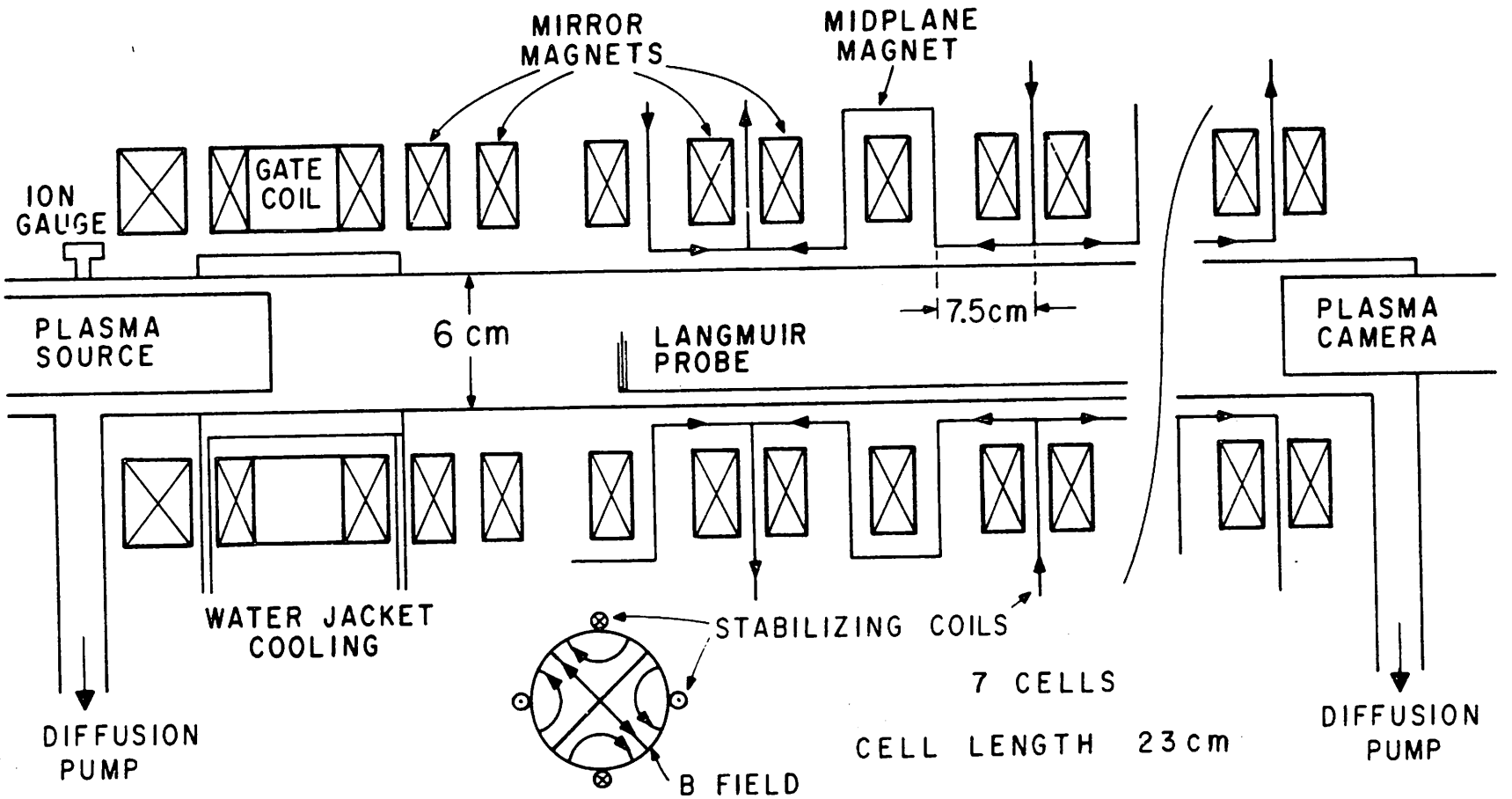


FIGURE 8 Schematic of multiple mirror device including quadrupole windings.

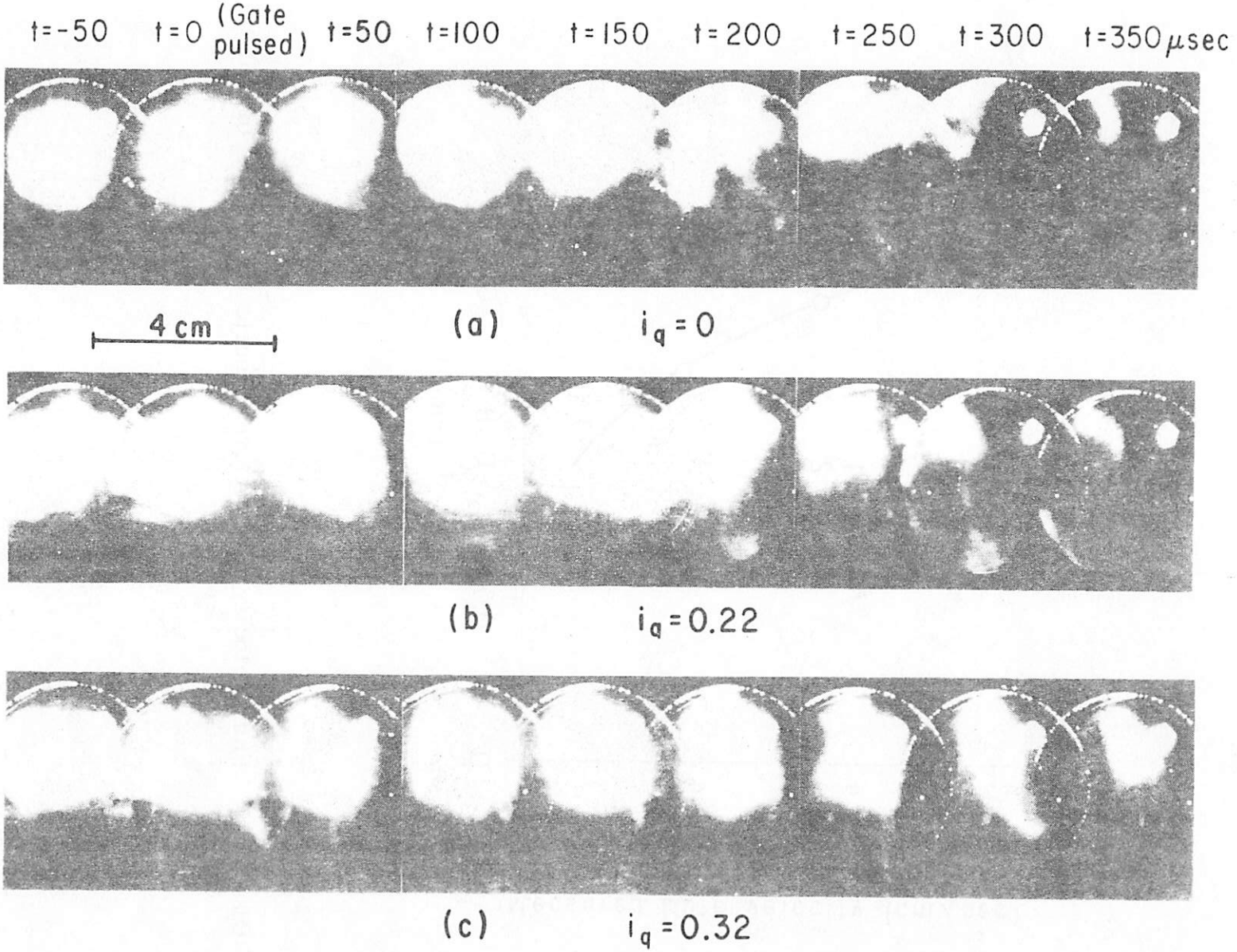


FIGURE 9 Time evolution of the thermal lithium plasma for $M = 4.2$ and three values of stabilizing current $i_q$ .

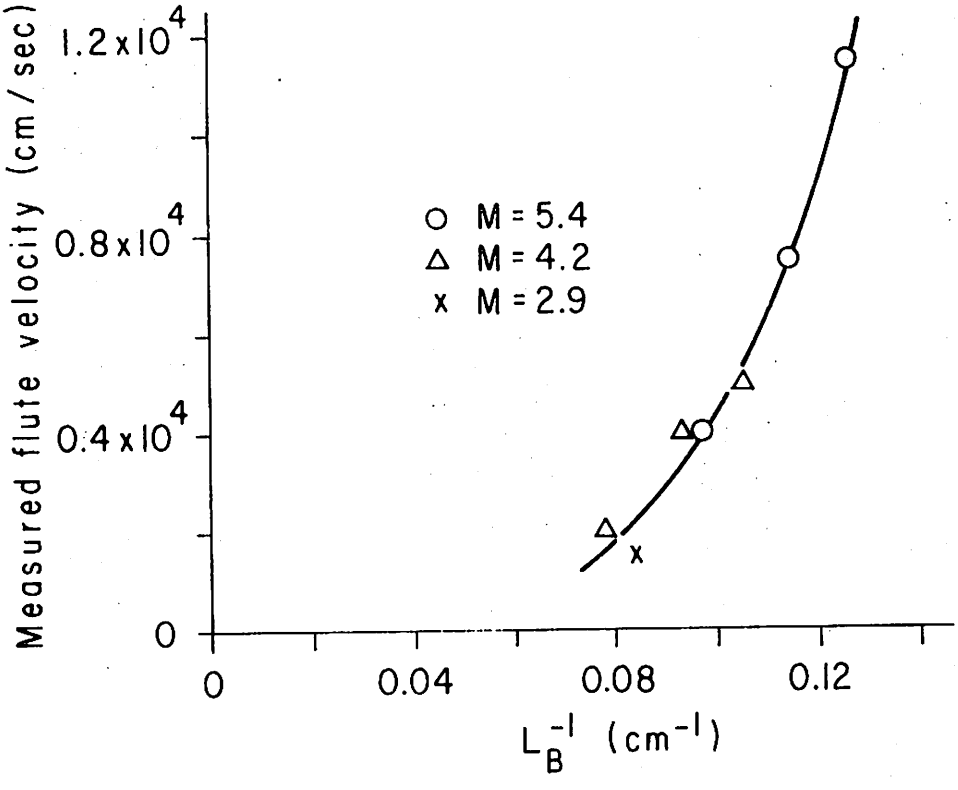


FIGURE 10 Flute velocity vs effective magnetic field scale length.

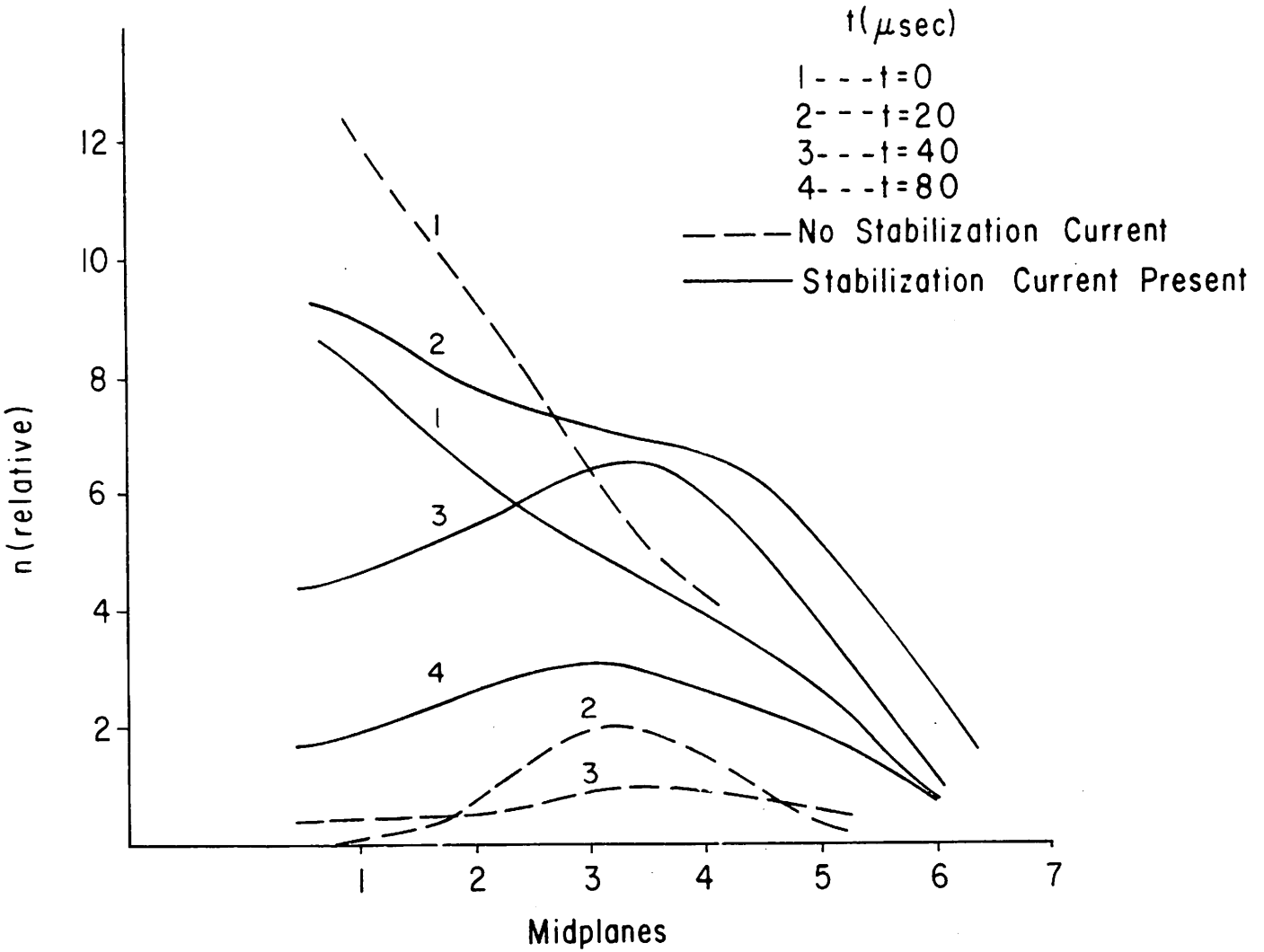


FIGURE 11 Decay of axial density in multiple mirror with and without stabilization ($\theta$ - pinch plasma source).

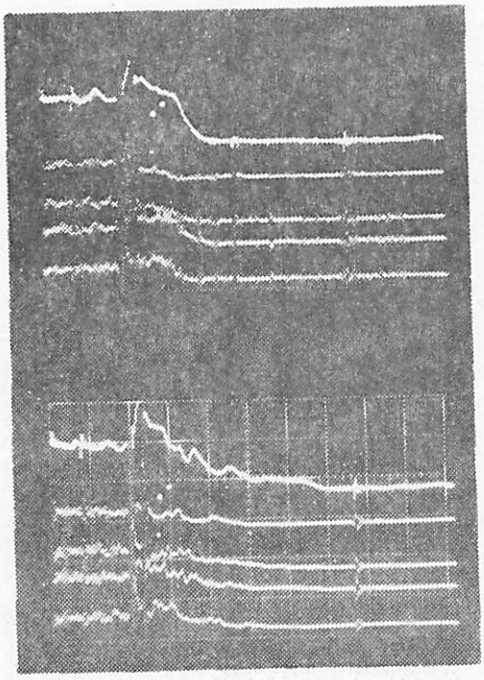


FIGURE 12 Typical Langmuir probe saturation currents vs time for axial integral feedback stabilization. Top trace: probe at r = 0. Bottom four traces: probes at r = 0.5 cm, 90° apart in azimuth. Timescale: 200 μsec/cm.

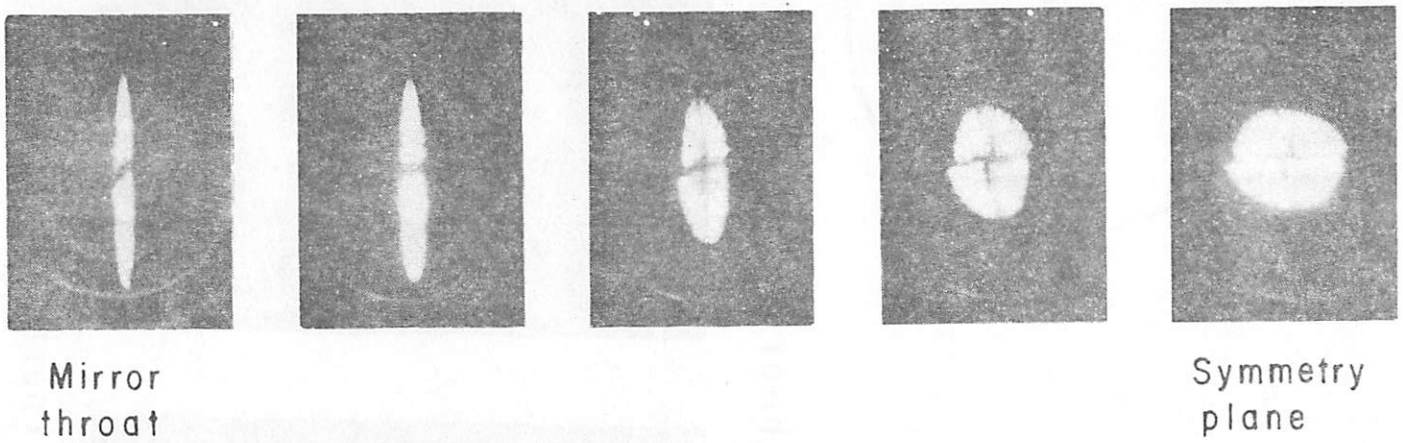


FIGURE 13a A series of plasma camera photographs of the flux surfaces as traced out by an electron beam from the mirror throat of a cell to the symmetry plane near the cell midplane. The distortion has not been fully compensated in this sequence.

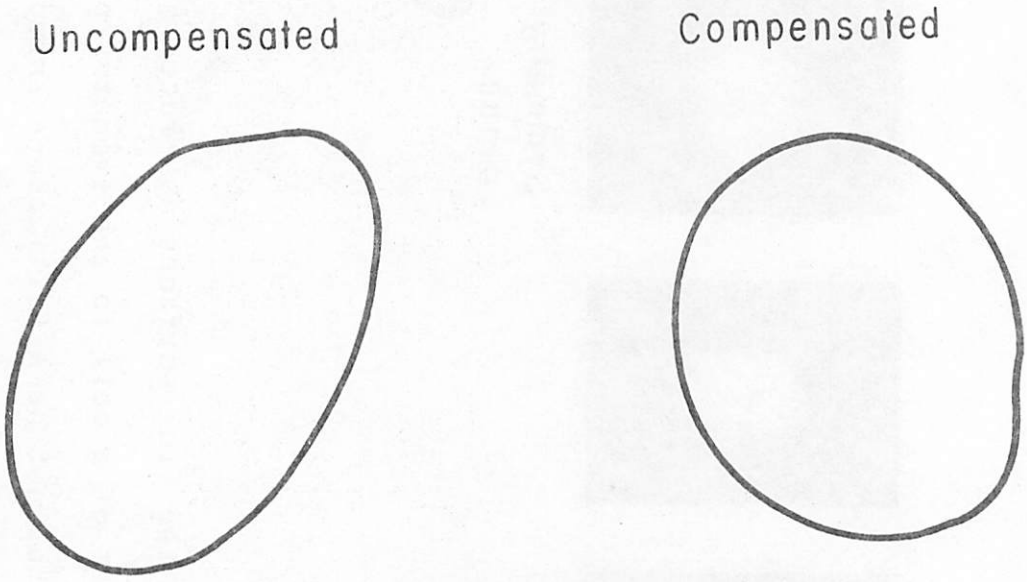


(a) Theory

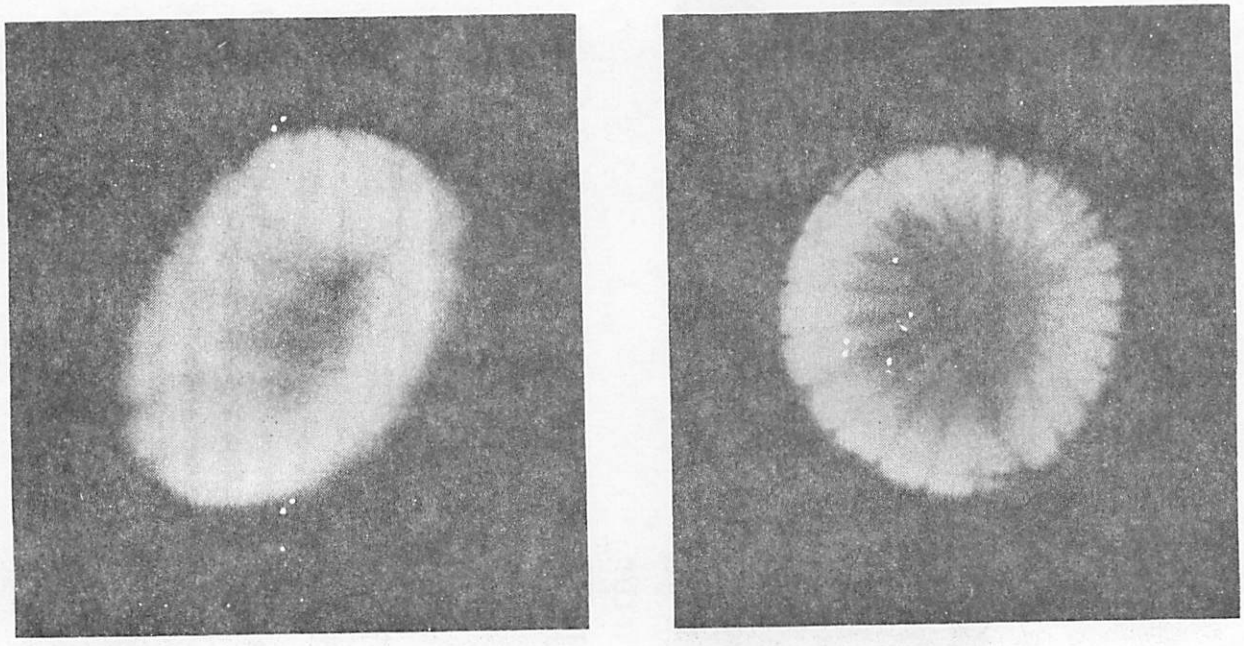

(b) Experiment

FIGURE 13b Theoretical flux surfaces (a) and experimental flux surfaces (b), measured using a low voltage electron beam and a "plasma camera" illustrating the correction of dipole distortion. The experiment has been enlarged by a factor of 4.

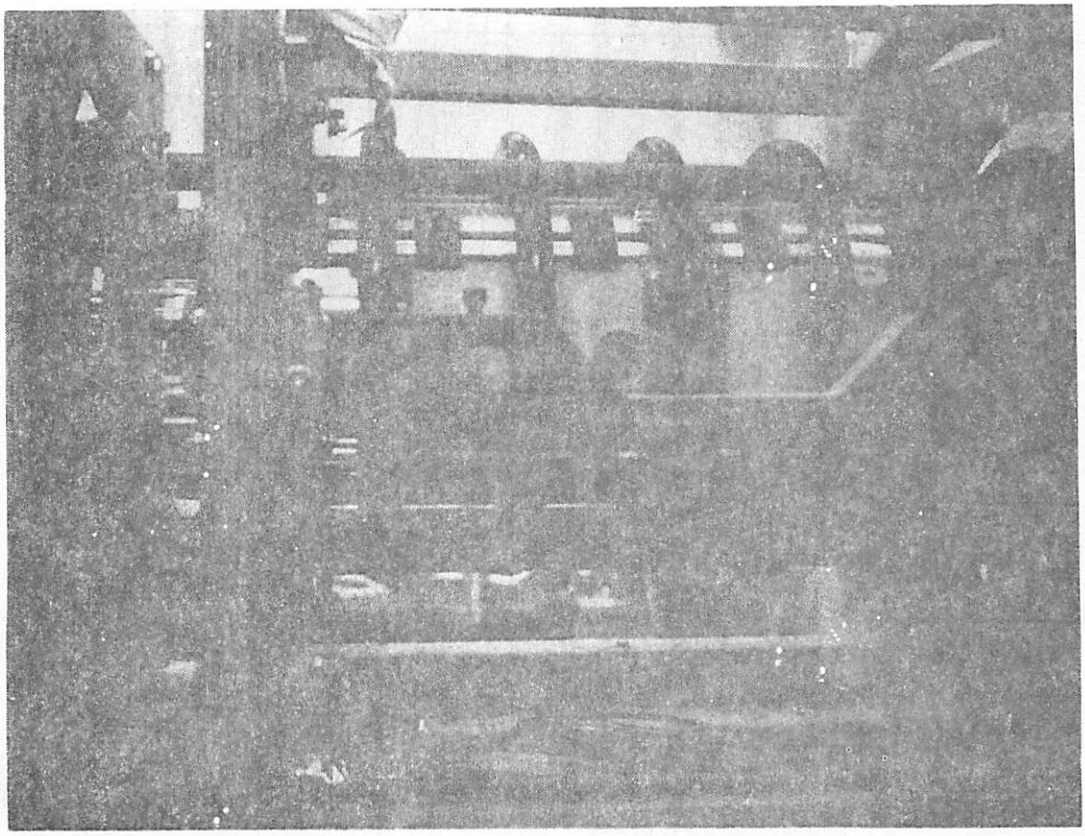

FIGURE 14 A single multiple mirror cell. The two midplanes are at the ends, with the min-ave-B mirror strong quadrupole windings embedded inside the epoxy-fiberglass cylinder in the center of the cell. The weak quadrupole bars are attached to the outside of the cylinder, and are surrounded by the seven turns of the solenoid.

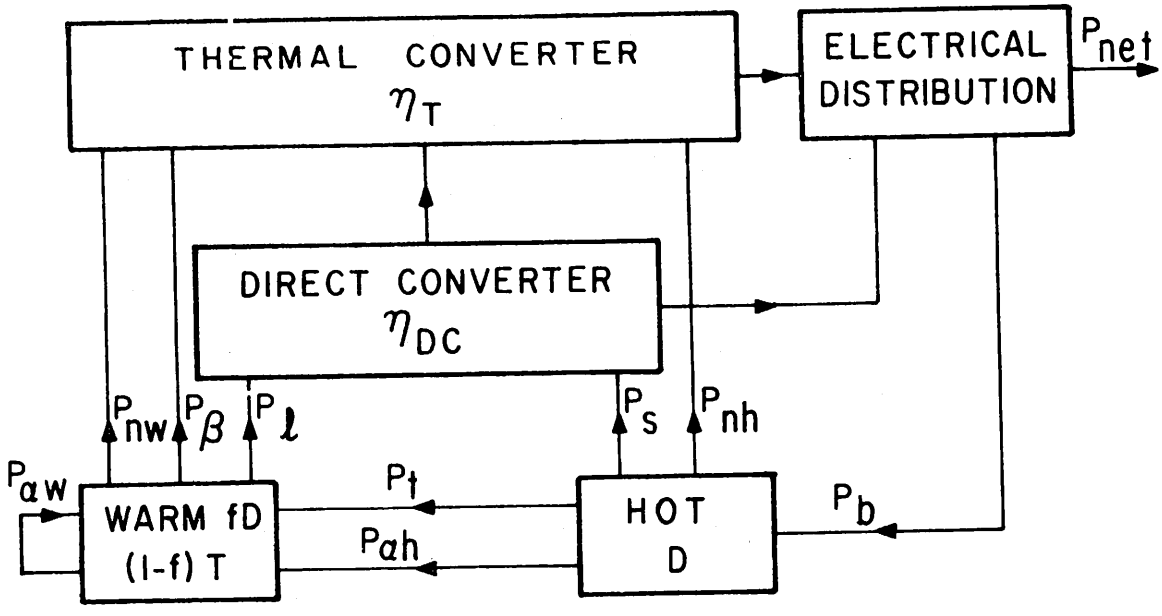


FIGURE 15 Power flows for a two-component multiple mirror reactor.

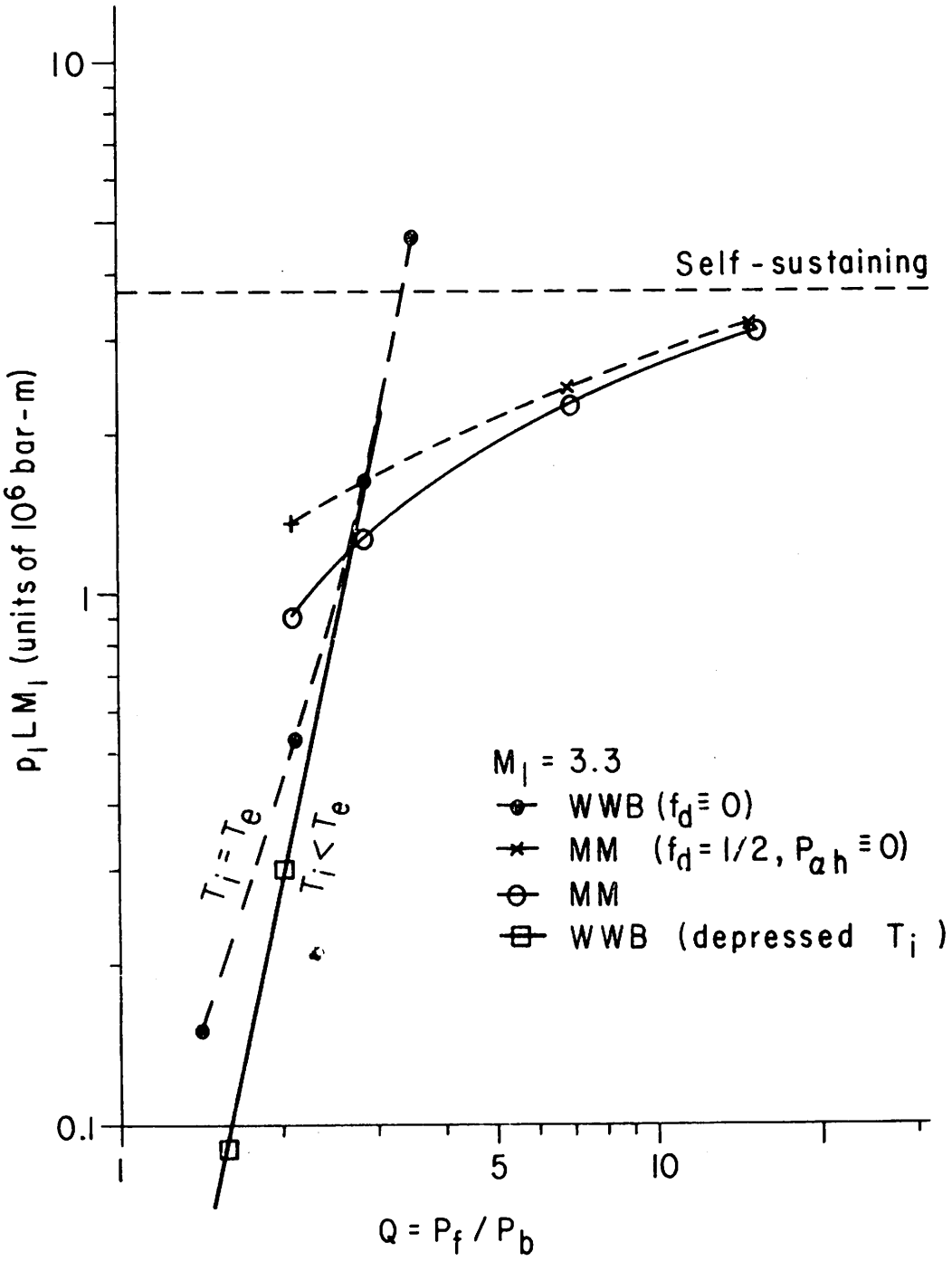


FIGURE 16 Pressure-length-mirror ratio $p_1 LM_1$ vs Q for a wetwood burner (WWB), a multiple mirror reactor without injected beam MM($f=\frac{1}{2}$, $P_h = 0$), and a multiple mirror reactor with injected beam MM (f optimized), for $M_1 = 3.3$.

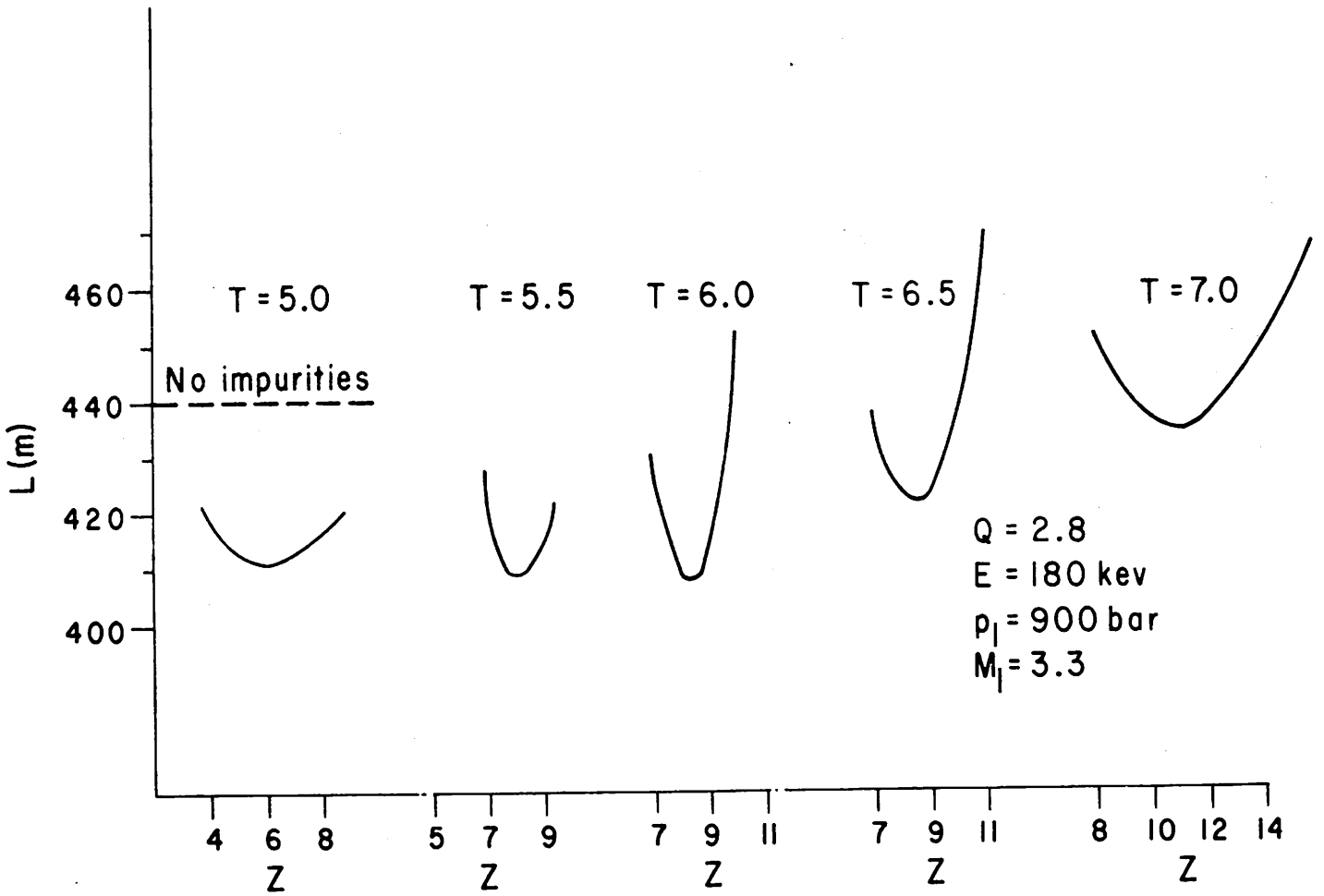


FIGURE 17 The reduction in length L for different temperatures T, due to the presence of a fraction $f_z$ of a fully stripped impurity of atomic number Z in the warm component. $Z^2 f_z$ effects alone are considered, with Q = 2.8, $p_1$ = 900 bars and $M_1$ = 3.3.